Journal of South American Earth Sciences 111 (2021) 103479

Contents lists available at ScienceDirect

Journal of South American Earth Sciences

journal homepage: www.elsevier.com/locate/jsames

A reinterpretation of pyroclastic density current deposits at Copahue volcano, Andean Southern Volcanic Zone, Argentina-Chile

Alejandro D. Báez [a,b,*], Walter Báez [c], Alberto T. Caselli [a,b], Romina Daga [d,e], Carlos A. Sommer [f]

[a] Universidad Nacional de Río Negro, Instituto de Investigación en Paleobiología y Geología, Río Negro, Argentina
[b] Consejo Nacional de Investigaciones Científicas y Técnicas (CONICET), Instituto de Investigación en Paleobiología y Geología, Río Negro, Argentina
[c] IBIGEO (Universidad Nacional de Salta-CONICET), Av. Bolivia, 5150, A4400FVY, Salta, Argentina
[d] Laboratorio de Análisis por Activación Neutrónica, Centro Atómico Bariloche, Comisión Nacional de Energía Atómica, Bariloche, Argentina
[e] Centro Científico Tecnológico, CONICET, Patagonia Norte, Argentina
[f] Universidade Federal do Rio Grande do Sul (UFRGS), Av. Bento Gonçalves 9500, 15001, 91501-970, Porto Alegre, Brazil

ARTICLE INFO

Keywords:
Caviahue-Copahue Volcanic Complex
Glaciovolcanism
Mixed avalanches
Clastogenic lavas
Volcanic hazards

ABSTRACT

Pyroclastic density currents (PDCs) are one of the most dangerous volcanic phenomena. The correct interpretation and mapping of PDC deposits in the volcano record is important to establish the eruptive style and play a fundamental role in hazard assessment and risk management. The Copahue volcano is an active intermediate volcano of the Southern Volcanic Zone of the Andes (Argentina-Chile) that presents fragmentary evidence of explosive activity during its evolution, with unusual minor PDC deposits. The recorded historic eruptions were mainly phreatomagmatic due to the presence of a crater lake. In this study, four key deposits previously interpreted as PDC products corresponding to different stages of the Copahue volcano evolution (Pleistocene, Holocene, and Historic times) are analyzed and this origin is discussed: (i) A Pleistocene reddish succession located in the northeast flank of the volcano formed by stretched bombs in a coherent lava is interpreted as clastogenic lavas; (ii) a series of proximal bedded volcaniclastics deposits of Pleistocene age are interpreted as redeposition of hyaloclastic fragments from syn-eruptive subglacial meltwater flows associated with subglacial eruptions; (iii) a distal Holocene deposit located ~12 km east of the active crater consist mainly in fine-sized clasts forming aggregates is reinterpreted as a sedimentary (lacustrine) deposit with volcaniclastic input; and, (iv) a historic whitish-grey clastic deposit located on the eastern flank is considered a product of a mixed avalanche generated during the 1992–1995 activity. Consequently, the PDC occurrence during the Copahue volcano evolution is less than previously thought. Large PDCs are unlikely in the future and their influence area would be reduced near the active crater as observed in recent eruptions. Flows triggered by the melting of snow/ice during volcanic activity and sudden drainage of the crater lake appear to be a more likely potential hazard that should be considered during risk assessment.

1. Introduction

Explosive volcanic activity is one of the most amazing natural phenomena and it is potentially destructive and capable of causing devastating societal impacts (e.g. Houghton, 2015; Cassidy et al., 2018). It can be generated by purely magmatic mechanisms (Cashman and Scheu, 2015) or by the interaction of magma with external water (Houghton et al., 2015). Explosive eruptions can lead to the generation of pyroclastic density currents (PDCs), which are one of the most dangerous volcanic phenomena and the main cause of death by volcanic activity worldwide, at least since 1600 CE (Witham, 2005; Auker et al., 2013). PDCs are inhomogeneous mixtures of pyroclastic particles and gas that flow under the influence of gravity and present a continuum from dilute to concentrated members given by the ratio between the solid and the fluid phases (Branney and Kokelaar, 2002; Sulpizio et al., 2014). This spectrum is reflected in a diverse range of PDCs deposits that record the processes and conditions of the lowermost part of the current denominated flow-boundary zone (Branney and Kokelaar, 2002; Sulpizio et al., 2014). PDCs deposits vary from massive to stratified and can share common features with other volcaniclastic or sedimentary deposits, making their correct interpretation often difficult (Moorhouse and White, 2016).

* Corresponding author. Universidad Nacional de Río Negro, Instituto de Investigación en Paleobiología y Geología, Río Negro, Argentina.
E-mail address: adbaez@unrn.edu.ar (A.D. Báez).

https://doi.org/10.1016/j.jsames.2021.103479
Received 17 March 2021; Received in revised form 15 July 2021; Accepted 15 July 2021
Available online 17 July 2021

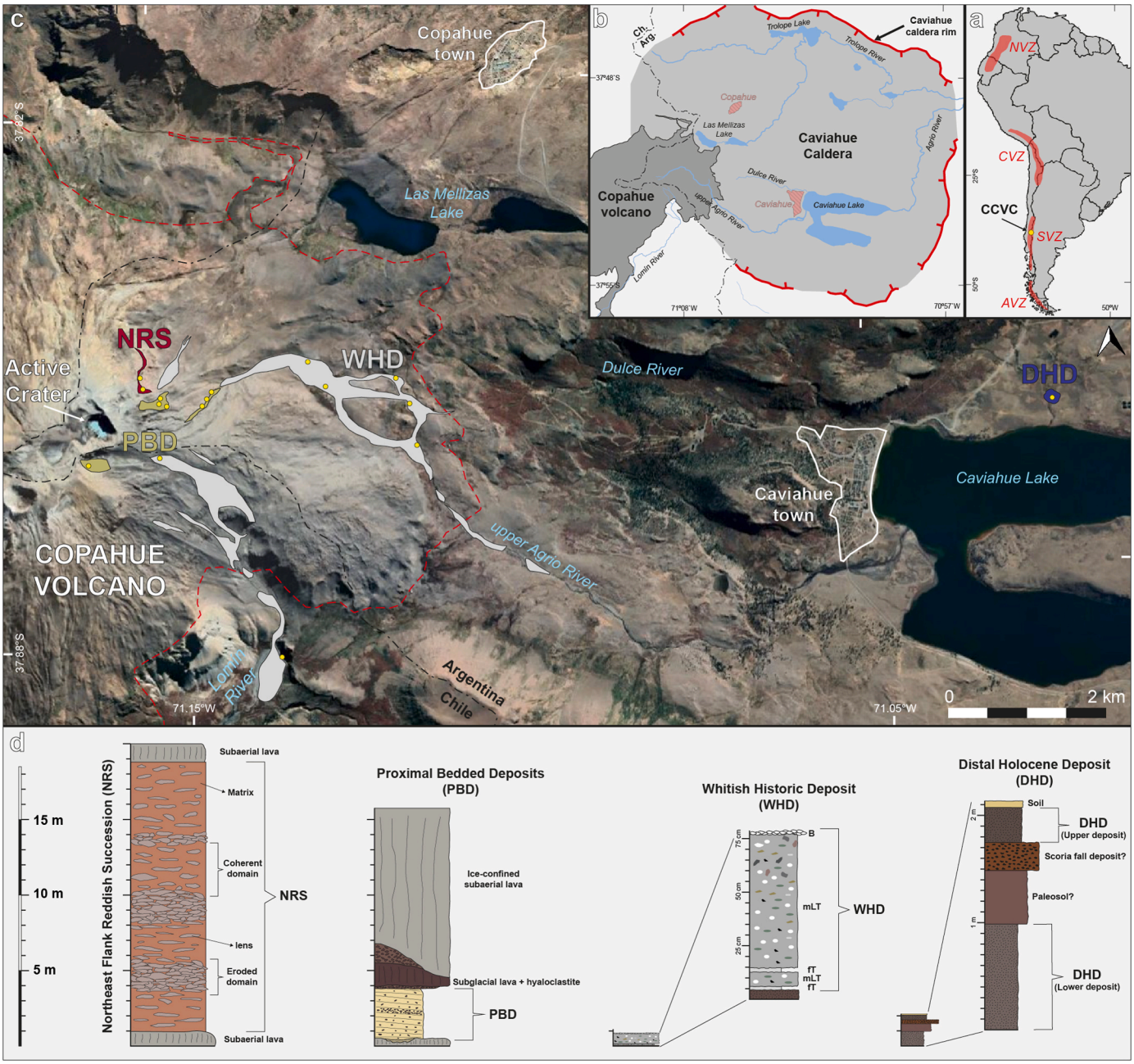

Fig. 1. Location maps. **a.** The South American continent map showing the distribution of the Andean Volcanic Zones (Austral Volcanic Zone (AVZ), Southern Volcanic Zone (SVZ), Central Volcanic Zone (CVZ), and Northern Volcanic Zone (NVZ)) with the location of the Caviahue-Copahue Volcanic Complex (CCVC). **b.** The Caviahue caldera map showing the location of the Copahue volcano in the western rim of the caldera, and the location of the Argentinian towns of Caviahue and Copahue inside the caldera. **c.** Satellite image of the Copahue volcano with the location of the analyzed deposits (NRS: Northeast Flank Reddish Succession; PBD: Proximal Bedded Deposits; DHD: Distal Holocene Deposit; WHD: Whitish Historic Deposit). The red dashed line indicates the limit of the Copahue volcano, and the yellow circles indicate the location of the sampling stations. **d.** Schematic stratigraphic logs of the analyzed deposits (B: blocks; mLT: massive lapilli tuff; fT: fine tuff).

Copahue volcano (37.86°S, 71.17°W; Argentina-Chile) is an active intermediate volcano of the Southern Volcanic Zone of the Andes (Fig. 1a). It is emplaced on the western rim of the Plio-Pleistocene Caviahue caldera, forming together the Caviahue-Copahue Volcanic Complex (Linares et al., 1999) (Fig. 1b). The Copahue volcano has an elongated SW-NE shape with several craters aligned in the summit, of which the easternmost is currently active and host of an acidic crater lake inside and two acidic hot springs on its eastern flank (Varekamp et al., 2001; Agusto and Varekamp, 2016). Also, the volcano summit hosts a small glacier that feeds the crater lake, and the entire edifice is covered by a significant snow cap during the winter season.

The Copahue volcano is at least younger than ~1.25 Ma (Linares et al., 1999) and evidence of explosive activity during its evolution is fragmentary with unusual minor PDCs deposits mentioned in the literature. The explosive character observed in the eruptive activity in the last three decades is mainly a consequence of the interaction with the hydrothermal system (Delpino and Bermúdez, 1993; Naranjo and Polanco, 2004; Petrinovic et al., 2014b; Caselli et al., 2016a, 2016b, 2016b; Daga et al., 2017).

In this study, we reappraisal the significance of the generation of PDCs during the Copahue volcano evolution from the analysis and reinterpretation of four key deposits previously interpreted as PDCs products corresponding to different stages of the edifice evolution (Pleistocene, Holocene, and Historic times) (Fig. 1c and d). The correct

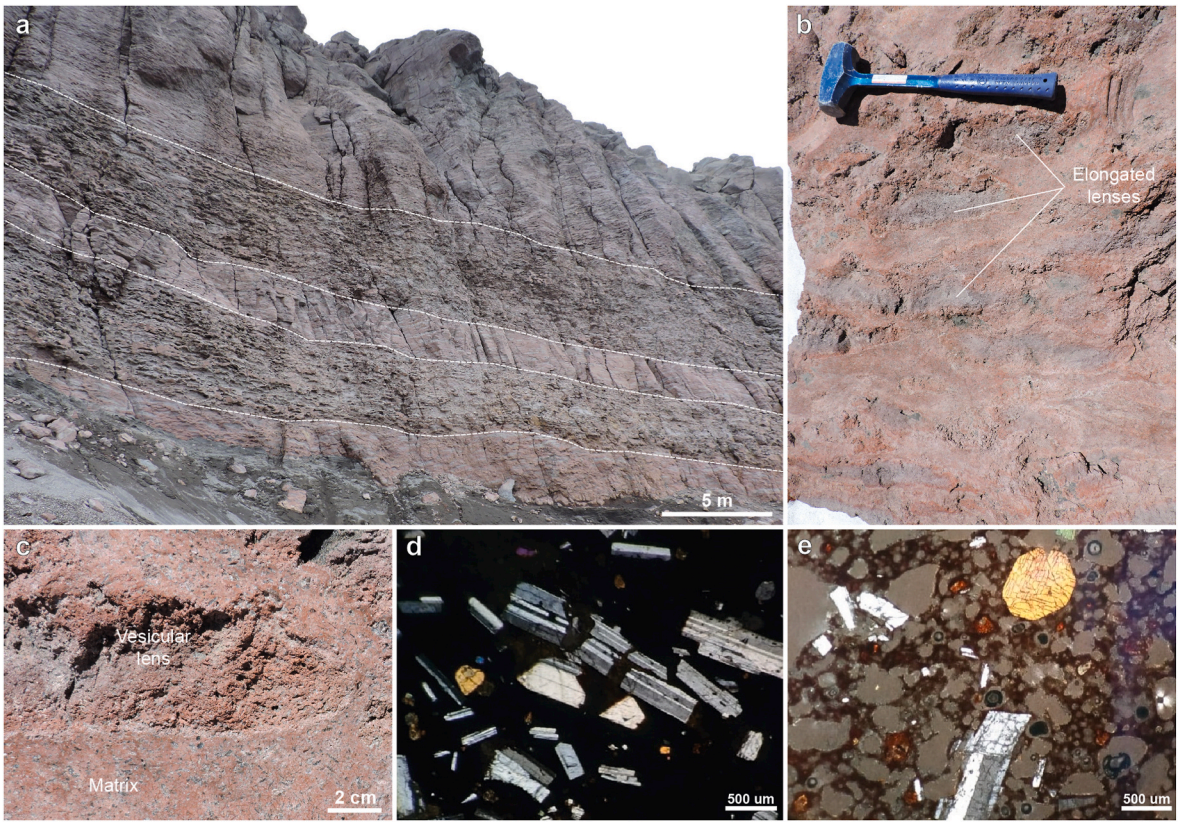

Fig. 2. General features of the Northeast flank Reddish Succession (NRS). **a.** Overview of the reddish wall formed by the NRS. Note the alternation between coherent and eroded domains. **b.** Aspect of coherent areas showing oriented, elongated lenses in a red matrix. Hammer is 28 cm in length. **c.** Detail of the contact between the lenses and the matrix. **d.** Photomicrograph under cross-polarized light of the lava (matrix) with vitreous groundmass showing a broken plagioclase. **e.** Photomicrograph under cross-polarized light of vesicular lens showing plagioclase and clinopyroxene phenocrysts.

estimation of the style of volcanic activity and its associated processes plays a fundamental role in the hazard assessment and risk management of the Copahue volcano. This is extremely important considering that the Argentinian towns of Caviahue and Copahue are located 9.5 km and 5 km from the active crater.

2. Explosive activity of Copahue volcano

Evidence of Pleistocene explosive activity comprises only the mention of minor PDC deposits without detailed descriptions of them (Melnick et al., 2006; Sruoga and Consoli, 2011; Forte and Caselli, 2014; Caselli et al., 2016a). During Holocene times, the SW-NE-aligned summit craters were formed in association with the generation of small PDCs (Delpino and Bermúdez, 1993, 1994, 1994; Melnick et al., 2006). Polanco (1998, 2003) described six PDC deposits distributed in the surroundings of the Copahue volcano in Chilean and Argentine territory, and groups them within the unit "*Depósitos Piroclásticos Copahue*". Radiocarbon dating on these deposits yields ages between 8.770 ± 70 BP and 2.280 ± 50 BP (Polanco, 1998). Based on the ages obtained, a recurrence rate of explosive activity of 650–700 years was estimated (Polanco et al., 2000). A possible historical dilute PDC deposit located just east of the active crater is mentioned by Báez et al. (2020).

In historic times, 10 eruptions have been reported (1750, 1759, 1867, 1876, 1937, 1944, 1960–1961, 1992–1995, 2000, 2012–2021), most of them corresponding to phreatic and phreatomagmatic activity (Petit-Breuilh, 2004; GVP, 2013; Caselli et al., 2016a; Caselli, pers. comm.). However, only 1992–1995, 2000, and 2012 eruptions have detailed descriptions.

The 1992–1995 activity cycle consisted of low-magnitude phreatic-phreatomagmatic eruptions characterized by eruptive columns smaller than 1500 m height and the occurrence of several lahars (Delpino and Bermúdez, 1993; Bermúdez and Delpino, 1995).

The 2000 eruption also began with phreatic-phreatomagmatic explosions, but then changed to a strombolian activity when the crater lake was completely emptied (Delpino and Bermúdez, 2002; Naranjo and Polanco, 2004). During the most intense stages, the eruptive column reached up to 2000 m height, a small lahar that traveled <2 km along the upper Agrio river was generated, and only small dilute PDCs were formed on the northern and eastern flanks (Delpino and Bermúdez, 2002; Naranjo and Polanco, 2004). Fish mortality due to a decrease in pH values of the water was mentioned for the Lomín river, although no lahars was registered (Naranjo and Polanco, 2004).

A small phreatomagmatic explosion during July 2012 begins the most recent eruptive cycle (Daga et al., 2017), which presented its largest eruption on December 22, 2012. Similar to the 2000 eruption, this eruption changed from a phreatic-phreatomagmatic activity to a strombolian style, the eruptive column reached up to 2000 m height, and small dilute PDCs were observed near the crater (Petrinovic et al., 2014b; Caselli et al., 2016b). New minor magmatic eruptive events were recorded in the following years, even up to the date of presentation of this contribution (March 2021) (Caselli et al., 2018; Caselli, pers. comm.)

3. Methods

In this work, we use a multiproxy approach to determine the origin of the analyzed deposits. Fieldwork was carried out between 2015 and 2019 and consisted of conventional volcanic stratigraphy field studies (stratigraphic logging, detailed description of the lithofacies, collection of samples, etc.). The volcaniclastic deposits (including syn-eruptively

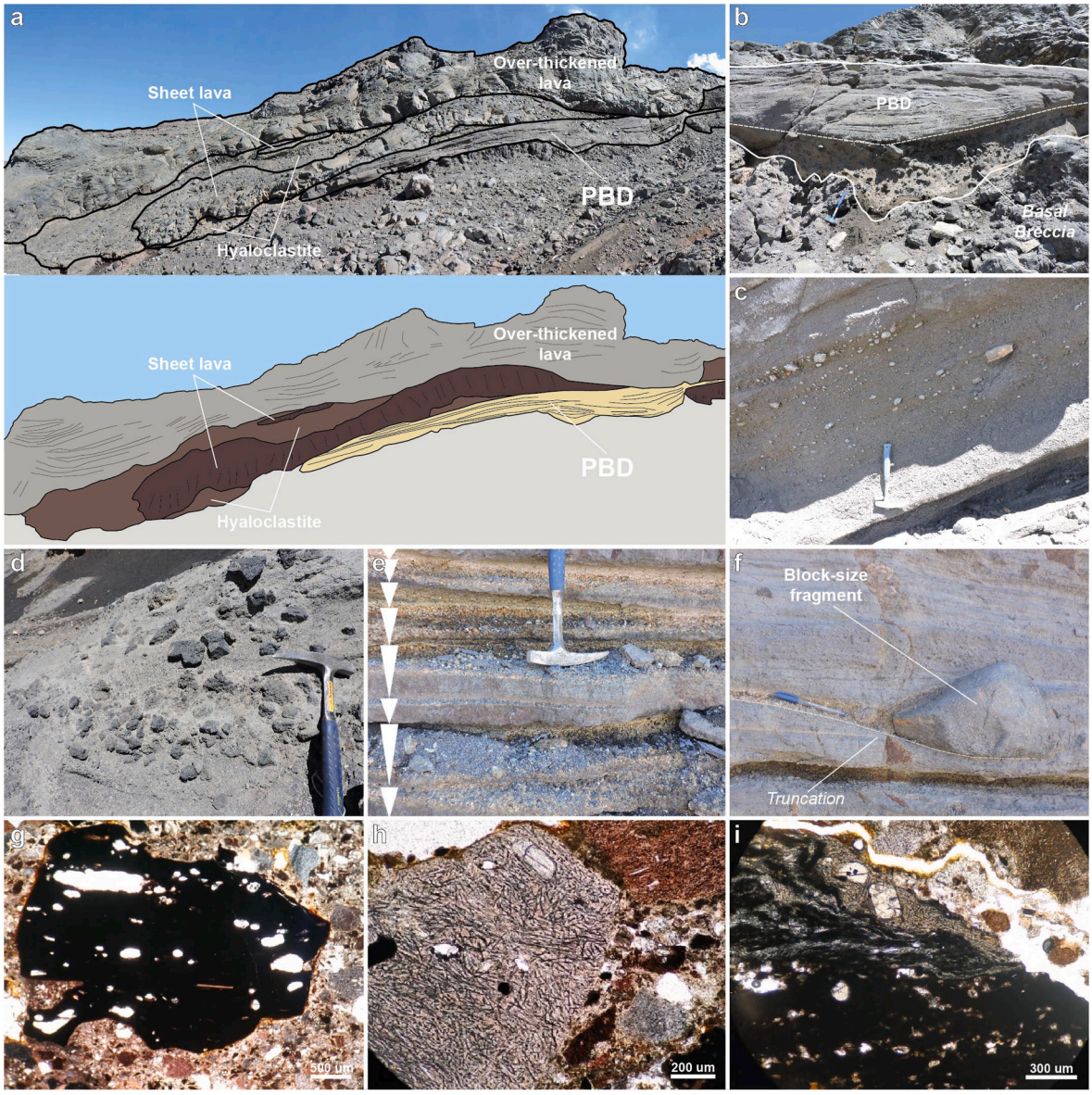

Fig. 3. General features of the Proximal Bedded Deposits (PBD). **a.** Panoramic view of the PBD and the associated lavas located ~500 m east of the active crater (top), and sketch of the same area (bottom). Field of view ~100 m. **b.** Matrix-supported basal breccia locally preserved. Hammer is 28 cm long. **c.** Massive to crudely bedded lapilli tuff with few blocks. **d.** Tuff breccia lithofacies. **e.** Rhythmic alternation of inversely grade beds. In figure d and e the hammer is 33 cm long. **f.** Scour and fill structure in clast-supported bed, and truncation of the underlying beds. Note the block-size fragment without sags structures. **g.** Clast of vesicular black glass with palagonitized rims. **h.** Clast of pale glass with several acicular opaques microlites. **i.** Clast showing the transition between black glassy domain and pale glassy with acicular microlites domain. Figs. g–i are photomicrographs under plane-polarized light.

redeposited deposits) are described using the terminology proposed by White and Houghton (2006).

The petrographic analysis consisted of the study of thin sections under the petrographic microscope or under the binocular loupe, depending on the nature of the sample. To determine the granulometric distribution, some volcaniclastic samples were sieved using a Ro-Tab sieve shaker. Statistics parameters were calculated using the Folk and Ward (1957) method through the program GRADISTAT (Blott and Pye, 2001).

Supplementary estimation of the content of organic matter was realized by loss of ignition (LOI) in 1-g samples at 550 °C for 4 h (Heiri et al., 2001). The SEM-EDS analysis was carried out in a Philips SEM 515 scanning electron microscope, and a SEM-FEG FEI Nova Nanosem 230 in the *Centro Atómico Bariloche* (*Departamento de Caracterización de Materiales*, CNEA), Argentina. Bulk mineralogy was analyzed by X-ray diffraction (XRD) with a PANalytical X-ray diffractometer operated at 30 mÅ and 40 kV at the *Departamento Caracterización de Materiales* (*Centro Atómico Bariloche*, Argentina), collecting data from 5° to 60° 2θ. LandSat 4–5 TM imagery was obtained from the USGS Global Visualization Viewer (GloVis) development by the United States Geological Survey (https://glovis.usgs.gov/).

4. Analysis of the deposits

In this section, we analyze four key deposits previously interpreted as PDC products, named here as Northeast Flank Reddish Succession (NRS), Proximal Bedded Deposits (PBD), Distal Holocene Deposit (DHD), and Whitish Historic Deposit (WHD). These correspond to different stages of the edifice evolution, including Pleistocene (NRS and PBD), Holocene (DHD), and Historic times (WHD). Pleistocene deposits are volumetrically larger than the younger ones, although the latter are preserved in more distal positions. Each sub-section below corresponds

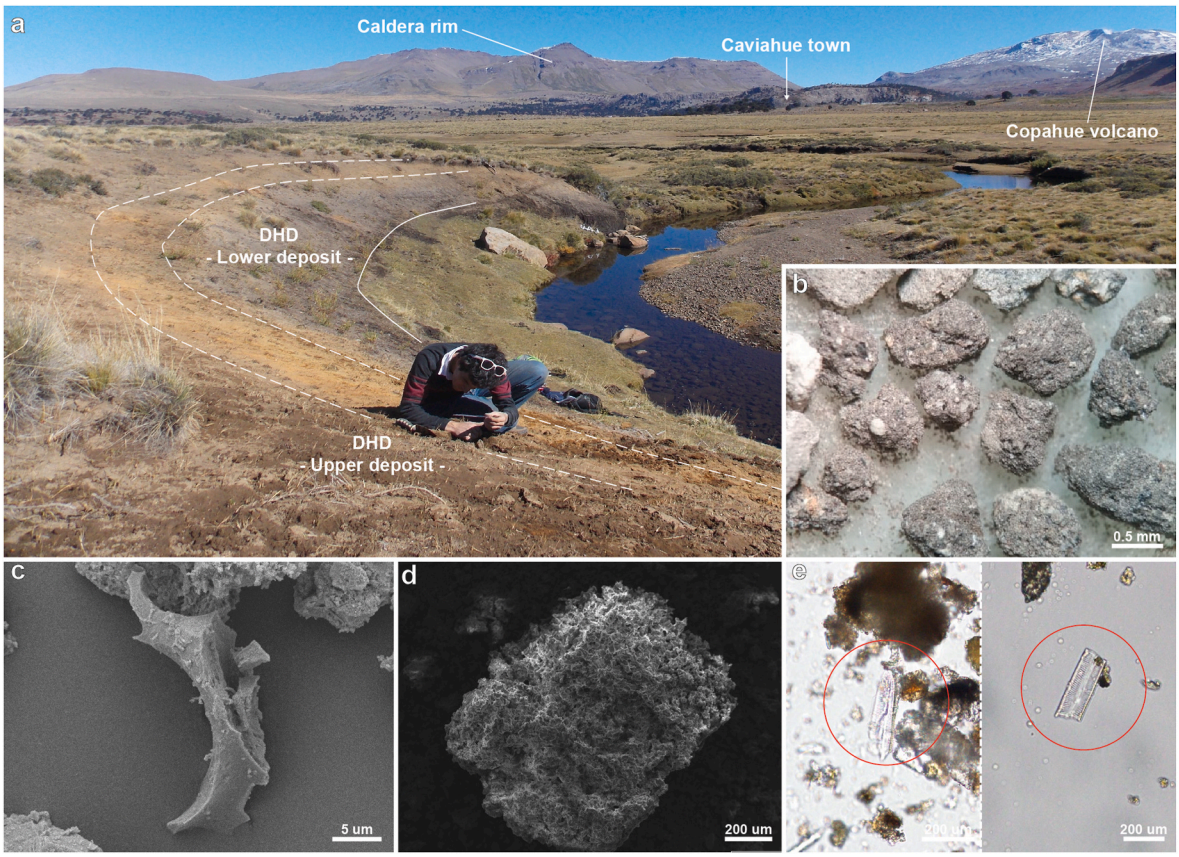

Fig. 4. General features of the Distal Holocene Deposit (DHD). **a.** Overview of the DHD ~12 km east of the active crater. **b.** Photography of the 0 phi fractions of the sieved DHD showing aggregates. **c.** SEM image of fine cuspate glass shard. **d.** SEM image of fragment altered mainly to smectites. **e.** Fraction of the DHD in loose grains showing the presence of diatoms (red circle).

to one of these deposits and includes its location, background, and description. The discussion of their interpretation is addressed in the following section. The name assigned to each deposit corresponds to a combination of location, age, and/or distinctive-feature descriptors. It is important to emphasize that these nomenclatures do not correspond to new formational names and are only intended to quickly differentiate and recognize the analyzed deposits (for a discussion of the stratigraphic scheme of the Copahue volcano see Báez et al., 2020).

4.1. Northeast Flank Reddish Succession (NRS)

Northeast Flank Reddish Succession (NRS) refers to a distinctive reddish outcrop that forms a wall of ~20 m thick located ~500 m northeast of the active crater (Fig. 1). This sequence has been previously defined as a welded ignimbrite of Pleistocene age (Forte and Caselli, 2014; Caselli et al., 2016a). No detailed analysis supports this interpretation and only the presence of a massive welded fluidal texture has been mentioned (Forte and Caselli, 2014). Recently, Báez et al. (2020) reinterpreted this sequence as a succession of clastogenic lavas.

The NRS forms a distinctive reddish wall with vertical transitional intercalations between coherent domains and eroded domains (Fig. 2a). The coherent domains show a welded fluidal aspect composed of greyish elongated vesicular lenses in a coherent red (black in the fresh face) matrix (Fig. 2b). The eroded domains consist of similar components but with a predominance of vesicular lenses and scarce matrix.

The red/black matrix consists of a non-vesicular lava composed of an aphanitic groundmass that contains plagioclase and clinopyroxene phenocrysts up to 5 mm in length (Fig. 2c). The groundmass is vitreous to cryptocrystalline and contains microphenocrysts of plagioclase and clinopyroxene. In some sectors variation in microlites content evidence relicts of individual clasts. The crystals are weakly to moderately oriented and generally broken (Fig. 2d). Some fine crystal corresponds to fragments of broken crystals.

The greyish lenses are easily recognizable flattened and stretched bombs oriented parallel to the base. These are moderate to highly vesicular with vesicles up to ~1 mm in diameter and contain plagioclase and clinopyroxene phenocrysts (Fig. 2e). The vertical axis of the lenses is < 20 cm thick, while the horizontal axis varies from centimetric to metric scale, forming flow-banded textures in sectors of higher deformation.

4.2. Proximal Bedded Deposits (PBD)

The Proximal Bedded Deposits (PBD) includes a set of downslope-dipping bedded volcaniclastic deposits emplaced up to 1500 m from the active crater and preserved under fractured lavas and hyaloclastites with evidence of lava/ice interaction (Fig. 3a). The three main outcrops are located ~500 m to the east of the active crater, on the valley of the upper Agrio River, and immediately south of the active crater (Fig. 1). The outcrop located in the upper Agrio River has been previously mentioned as a dilute PDC deposit of Pleistocene age (Sruoga and Consoli, 2011a; Forte and Caselli, 2014; Caselli et al., 2016a). Báez et al. (2020) described the PBD and reinterpreted them as deposits emplaced by subglacial meltwater drainage streams with a syn-genetic relationship with the emission of the overlying lava flows.

Two types of lavas associated with the PBD have been recognized. Thin fractured sheet lavas enclosed by massive hyaloclastite breccias generally lie above the PBD. The top hyaloclastite is better developed while the basal hyaloclastite is thinner and locally disappears. A transition between the hyaloclastite and the PBD is locally observed. The

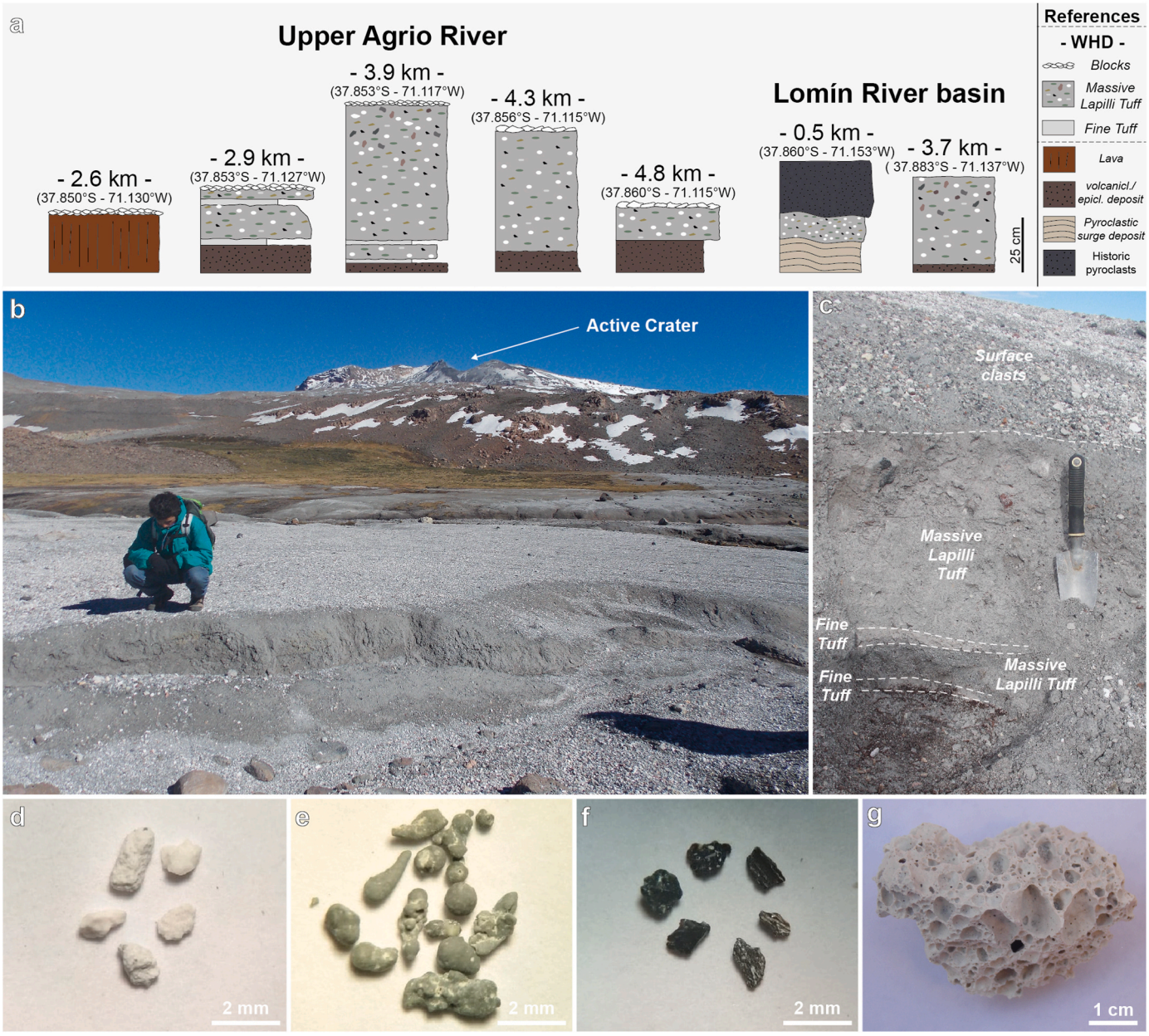

Fig. 5. General features of the Whitish Historic Deposit (WHD). **a.** Stratigraphic sections of the WHD in the upper Agrio River and the Lomín River basin. The distances are from the crater following the path of the deposit and its location coincides with the sampling stations in Fig. 1 **b.** Overview of the WHD showing greater thickness on flat slopes and thinner thickness without levees on the margins. **c.** Internal features of the WHD showing a main massive lapilli-tuff lithofacies with a thin basal fine tuff layer and a surface thin cap of block- and coarse lapilli-size clasts. A second similar underlying sequence is observed. **d-f.** Main components of the WHD: white fragments of amorphous silica (d), grey-greenish sulfur spherules (e), and poorly to moderately vesicular juvenile clasts (f). **g.** Whitish vesicular siliceous block present in the surface of the WHD.

sheet lavas are overlain by over-thickened lavas with steep margins and colling fractures. In some cases, these lavas cut the sheet lavas and rest directly in contact with the PBD. For more details of the cooling fractures present in these lavas see Báez et al. (2020).

The PBD consist of planar-bedded lapilli tuffs that are locally deformed, even showing large-scale slumps. A poor preserved matrix-supported basal breccia is locally observed (Fig. 3b). The main lapilli tuff consists of centimetric to decimetric individual beds defined by granulometric and clast/matrix ratio variation. Most of them consist of internally massive or crudely bedded beds dominated by coarse ash to fine lapilli-size subangular clasts and some coarse lapilli and isolated block-size fragments but without sags structures associated (Fig. 3c). Some beds present a higher content of blocks forming a matrix-supported tuff-breccia (Fig. 3d). The lack of fine-size components is persistent in the entire PBD.

Locally, the PBD presents a distinctive rhythmic alternation of centimetric beds that vary between moderately to well-sorted clast-supported beds composed by coarse ash to fine lapilli-size subangular to subrounded clasts, and matrix-supported beds consist in minor similar clasts in an ash-size matrix. In some cases, individual beds appear to vary between the matrix-supported to the clast-supported domains in the top, resulting in an inverse gradation (Fig. 3e). The clast-supported layers can cut to underlying beds (scour and fill structure) and present block-size fragments up to 30 cm but also without associated sags structures (Fig. 3f).

The PBD is mainly monomictic, with a predominance of subangular

dark grey to black lava fragments in the whole size range. These fragments have a porphyritic texture with phenocrysts of plagioclase in an aphanitic groundmass and are poorly to non-vesicular. Isolated yellow sulfur fragments of less than 5 cm also are present in the deposit.

In thin sections, three main clasts have been observed: (1) Black poorly vesicular glass with scarce plagioclase phenocrysts and palagonitized rims (Fig. 3g), (2) pale (transparent to yellowish-brown) vesicle-free glass with an undercooling texture that consists of several moderately oriented acicular opaque microlites and minor plagioclase microlites ranging from 25 μm to 100 μm, and some plagioclase and pyroxene phenocrysts (Fig. 3h), and (3) brown poorly vesicular glass with perlitic fractures, scarce plagioclase phenocrysts and palagonitized rims. In some cases, the contact between the black glass and the pale glass with acicular microlites is present in an individual clast (Fig. 3i). When a medium to fine ash-sized matrix is present, it consists of fragments compositionally like the higher clasts but with sizes between 0.1 and 0.5 mm thick, and without fine fragments <63 μm thick.

4.3. Distal Holocene Deposit (DHD)

The Distal Holocene Deposit (DHD) is located within the Caviahue caldera about ~12 km to the east of the active crater and ~350 m to the north of Lake Caviahue (37°51′40″ S - 71°1′23″ W) (Figs. 1 and 4a). It is exposed by erosion on the undercut bank of a stream that flows into the Caviahue lake.

The DHD is part of the Holocene deposits interpreted as products of PDCs by Polanco (1998, 2003). They are matrix-supported deposits up to 2 m thick formed mainly by fine-size components and with interbedded fall deposits (Polanco, 2003). The DHD includes two PDC deposits of 2 m and 1.2 m thick separated by a ~80 cm thick sequence formed by tephra-fall deposits, fluvial/lacustrine deposits, and paleosols (Polanco, 1998, 2003). The lower deposit is described as an organic-rich paleosol produced in a PDC deposit, whereas the upper deposit is described as an organic-rich PDC deposit (Polanco, 1998). Radiocarbon dating on the upper deposit of the DHD yields an age of 8770 ± 70 BP (Polanco, 1998).

In this contribution, a new stratigraphic section was made in the DHD and two main deposits were identified and correlated with the previously PDC deposits described by Polanco (1998, 2003). For the upper deposit, a maximum thickness less than that mentioned by Polanco (1998, 2003) was measured, although variations in its thickness were observed due to surface erosion.

Both the lower and the upper deposits present a massive aspect and are unconsolidated. Compositionally they are also similar and consist mostly of silt/clay-sized material that forms aggregates of up to ~5 mm (Fig. 4b). These aggregates are mainly composed of clay minerals and amorphous silica varieties. Black glass shards with poor to moderate vesicularity are present as isolated fragments up to 1 mm and forming part of the aggregates (Fig. 4c). Minor plagioclase and pyroxenes crystals and volcanic lithics are also present. White fragments altered to smectites and Fe–Ti oxides of up to 1 mm are also dispersed in the deposits (Fig. 4d). A white bed of 5 cm thick formed mainly by these white fragments is interspersed with transitional contacts in the lower deposit.

The organic matter content of both deposits is substantial, being 8.20% in the lower deposit and 11.65% in the upper deposit. Another relevant feature observed in both deposits is the presence of diatoms (*Bacillariophyceae*) confirmed by the analysis under the petrographic microscope of loose grains (Fig. 4e).

4.4. Whitish Historic Deposit (WHD)

The Whitish Historic Deposit (WHD) comprises a set of whitish-grey outcrops located along the drainages on the eastern flank of the volcanic edifice (Figs. 1 and 5a). The most significant outcrops are located in the Lomín and upper Agrio rivers reaching 4 km and 6 km long, respectively. Other minor outcrops are observed to the southeast and northeast of the active crater. Proximal deposits are currently not preserved or covered by pyroclasts from recent eruptions.

The detailed description of the August 1992 eruption mentions for August 2 the occurrence of grey ice-bearing lahars that traveled 4 km downstream into the upper Agrio river and 3.5 km into the Lomín river (GVP , 1992; Delpino and Bermúdez, 1993). During the September 12, 1995 eruption, a lahar of similar characteristics traveled 8 km into the upper Agrio river (Bermúdez and Delpino, 1995). The deposits of the 1992–1995 lahars were dark grey in color while wet and turned white when dried (Delpino and Bermúdez, 1993; Bermúdez and Delpino, 1995).

The distribution and general aspects of the WHD are the same as the 1992–1995 lahars, and subsequent contributions have attributed the WHD genesis to these lahars (Polanco, 2003; Sruoga and Consoli, 2011a). More recently, the WHD was interpreted as a product of PDCs generated during the 1961 eruption (Petrinovic et al., 2014a) and later attributed to the 2000 eruption (Balbis et al., 2016). Balbis et al. (2016) make a facies analysis and conclude that the lithofacies present in the WHD correspond to PDC deposits, pointing out that these cannot be the result of lahars. These authors also mention the presence of charred bushes within the deposit and the presence of the deposit adhered to the walls of the river valleys as evidence that support this interpretation. The proposed formation of the WHD during the 2000 eruption is based on the report of small dilute PDCs during the July 5, 2000 eruption (Naranjo and Polanco, 2004), and oral reports of the 2000 eruption from Caviahue inhabitants.

WHD distribution shows a strong topographic control during its emplacement. On flatter slopes, the deposit reaches up to 65 cm thick, whereas on steeper slopes and margins is only a few centimeters thick (Fig. 5b). The lack of marginal levees is present in the entire deposit. In the Lomín river the distal deposit presents a frontal lobe emplaced in a flat sector of the valley outside the edifice flank.

WHD consists of a grayish massive lapilli tuff very poorly sorted and clast-supported (Fig. 5c). The grain size mainly varies from very fine ash to medium lapilli, and with <5% of extremely fine ash matrix (<63 μm). The granulometric mean ranges between 1.5ϕ and −1.5ϕ, showing a platykurtic and coarse skewed distribution (see supplementary material). Few isolated coarse lapilli-sized clasts up to 5 cm are present in some locations towards the top of the deposit.

The lapilli tuff is polymictic and contains lithics (50–80%), and minor juvenile clasts (15–25%), and crystal fragments (<5%). The lithics consist of white sub-rounded fragments of crystalline silica varieties (tridymite + cristobalite + quartz) (Fig. 5d) and grey-greenish sulfur spherules (Fig. 5e). Minor proportions of yellow sulfur fragments and altered reddish volcanic lithics are also present. Juvenile clasts are grouped in black poorly to moderately vesicular glassy clasts with blocky texture and dark-brown to black moderately vesicular pumiceous clasts with vesicular textures and elongate vesicles (Fig. 5f). Crystal fragments are principally plagioclase and pyroxene.

Thin whitish layers (<2 cm) of fine tuff are also present at the base of the deposit in some sectors. This fine tuff is poorly sorted and mainly formed of extremely fine ash and very fine ash fragments, showing a very coarse skewed distribution (see supplementary material). The fragments in this lithofacies principally correspond to white silica lithics like the present in the lapilli tuff.

Isolated blocks up to 20 cm and coarse lapilli-size clasts lie on the surface of the deposits in several sectors. These clasts consist of whitish siliceous fragments with vesicular and massive textures composed of amorphous and crystalline silica varieties with the presence of sulfur and gypsum (Fig. 5g).

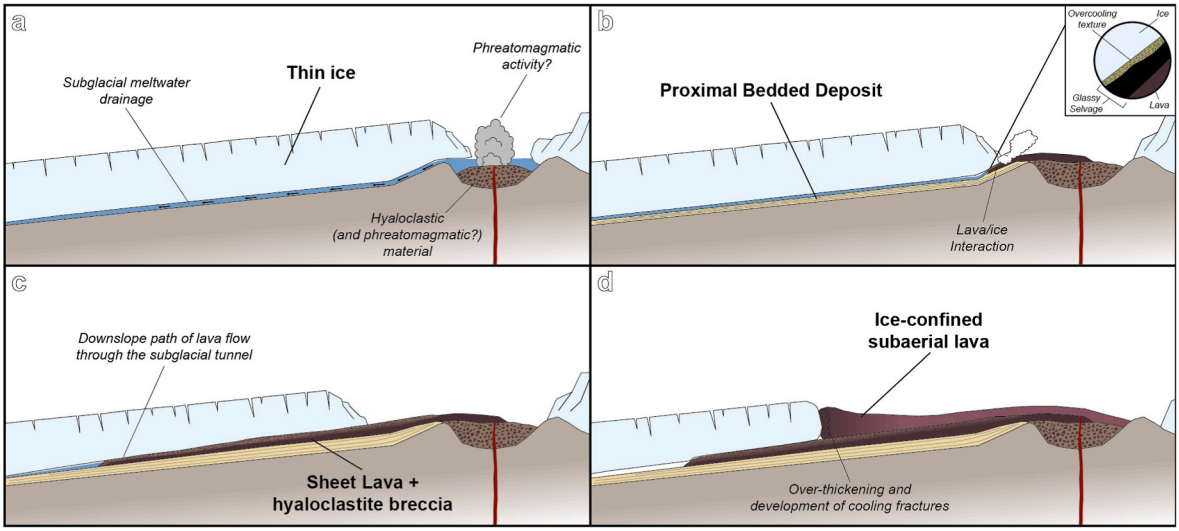

Fig. 6. Schematic illustration of the emplacement of the PBD and associated lavas/hyaloclastites. **a.** Initial subglacial to subaerial eruption with rapid and effective subglacial drainage of the meltwater. Possible generation of phreatomagmatic explosions. **b.** Emission of lava flow that interacts with the ice. Meltwater flow generates the PBD from the redeposition of the material generated in the eruption, mainly from the hyaloclastic fragmentation of the lava. **c.** The lava flow continues to advance below the glacier following the tunnels formed by the meltwater drainage flow. **d.** The glacial partially recedes due the volcanic/ice interaction allowing the emplacement of subaerial lava that is confined downslope by the ice.

5. Discussion

5.1. Origin of the deposits

5.1.1. Northeast Flank Reddish Succession (NRS)

Based on its textural characteristic and proximal location, we consider the NRS as a succession of clastogenic lavas, as previously proposed by Báez et al. (2020). These clastogenic lavas would have been formed during periods of high accumulation rates of fluid hot pyroclasts in a lava-fountain eruption.

Lava-fountains consist of sustained jetting of incandescent pyroclasts during Hawaiian eruptions, and its products include non-welded scoria cones, spatter piles and ramparts, and clastogenic lavas (Wolff and Sumner, 2000; Sumner et al., 2005). The latter are proximal lava flows formed by syn-depositional rheomorphic flow of agglutinated and coalesced hot pyroclasts (spatters), and show obvious fragments typically flattened, stretched, and deformed (Cas and Wrigth, 1987; Sumner, 1998; Wolff and Sumner, 2000). Internal textural variations from discernible agglutinate clasts to homogeneous lavas formed by coalesced clasts have been observed in clastogenic lavas (e.g. Sumner, 1998).

The red matrix of the NRS consists of entirely coalesced clasts with a total loss of vesicularity that forms quasi-homogeneous lava where obliterated clast outlines are difficult to recognize. This interpretation is also supported by the presence of a higher proportion of broken crystals than in a typical intermediate lava flow, indicating explosive activity prior to the formation of the lava flow (Yasui and Koyaguchi, 2004; Riggs and Duffield, 2008). The grey lenses consist of flattened and stretched pyroclastic bombs that preserve vesicularity, possibly corresponding to an outermost portion of the fountain (Sumner et al., 2005). The eroded areas with highest proportion of preserved bombs indicate a decrease in the clast accumulation rate and consequently in the degree of coalescence (Sumner et al., 2005).

Although lava-fountains represent the most frequent subaerial explosive eruption type (Sumner et al., 2005; Taddeucci et al., 2015), the formation mechanisms of fountain-fed clastogenic lavas are relatively poorly analyzed (Wolff and Sumner, 2000). However, in the last two decades the recognition and description of these type of lavas have increased (e.g. Riggs and Duffield, 2008; Carracedo Sánchez et al., 2012; Brown et al., 2014; Maro and Caffe, 2016; Yasui, 2017), and generation of clastogenic lavas have been reported in recent eruptions (e.g. Andronico et al., 2008; Waythomas et al., 2014; Frontoni et al., 2019), even in the Andean Southern Volcanic Zone (e.g. Romero et al., 2018; Vera, 2018).

5.1.2. Proximal Bedded Deposits (PBD)

The PBD show similarities with other sequences of bedded volcaniclastic deposits associated with hyaloclastites and lavas recognized in diverse glaciovolcanic environments (e.g. Smellie and Skilling, 1994; Smellie, 2008; Bennett et al., 2009; Banik et al., 2014; Lachowycz et al., 2015; Cole et al., 2018). In these sequences, the bedded volcaniclastic deposits have been interpreted as syn-eruptive redeposition of either hyaloclastic or phreatomagmatic clasts from subglacial meltwater flows.

Smellie (2008, 2013) defines subglacial volcanic sheet-like sequences as a combination of cogenetic volcanic (jointed lavas with evidence of ice/water interaction) and volcaniclastic lithofacies emplaced in a glacial eruptive environment that form tabular to ribbon-like outcrops with very low aspect ratios and steep margins. These represent sequences emplaced away from the vent and are predominantly basaltic (Smellie and Edwards, 2016), although examples of sequences with more evolved compositions exist (e.g. Edwards and Russell, 2002). Similar sequences with very narrow and sinuous morphologies that consist of jointed lavas and minor underlying volcaniclastic deposits interpreted as emplaced in subglacial tunnels have been called esker-like sequences and the distinction into a separate category from the sheet-like is uncertain (Smellie and Edwards, 2016).

Two types of sheet-like sequences (Mt. Pinafore and Dalsheidi types) have been distinguished based on subtle differences in lithofacies and architecture which would indicate different emplacement and coeval ice thicknesses (Smellie, 2008). Nevertheless, recent studies question this distinction arguing that the differences between the two types would be insufficient and the original interpretations have unresolved problems (Smellie and Edwards, 2016). In the more common Mt. Pinafore type, the volcaniclastic lithofacies include planar and cross stratified sand- and gravel-sized sediments, massive to crudely planar stratified hyaloclastite breccia, and in some cases a basal diamictite (Smellie and Skilling, 1994; Smellie, 2008). The former is interpreted as redeposited hyaloclastites and hyalotuffs by traction currents and hyperconcentrated flows formed by the meltwater generated during the eruptions that flushed away from the vent in tunnels beneath a thin glacial cover (Smellie, 2008; Smellie and Edwards, 2016). Overlying the

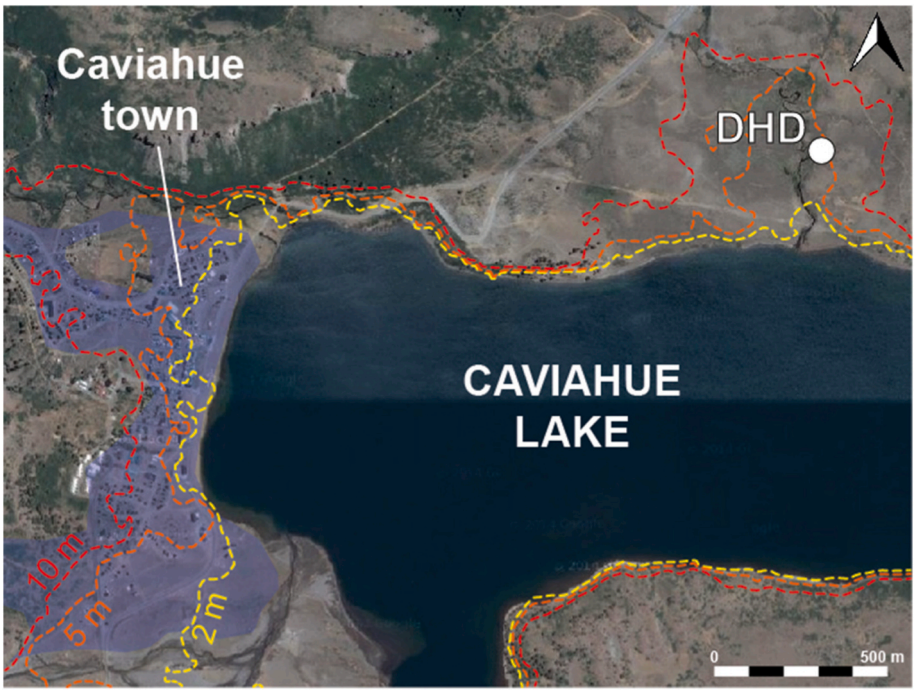

Fig. 7. Satellite image including the DHD and the Caviahue town. The dashed lines indicate the altitude (2 m, 5 m, and 10 m) above the current lake level. The blue shaded area is the lacustrine deposits from Melnick et al. (2006).

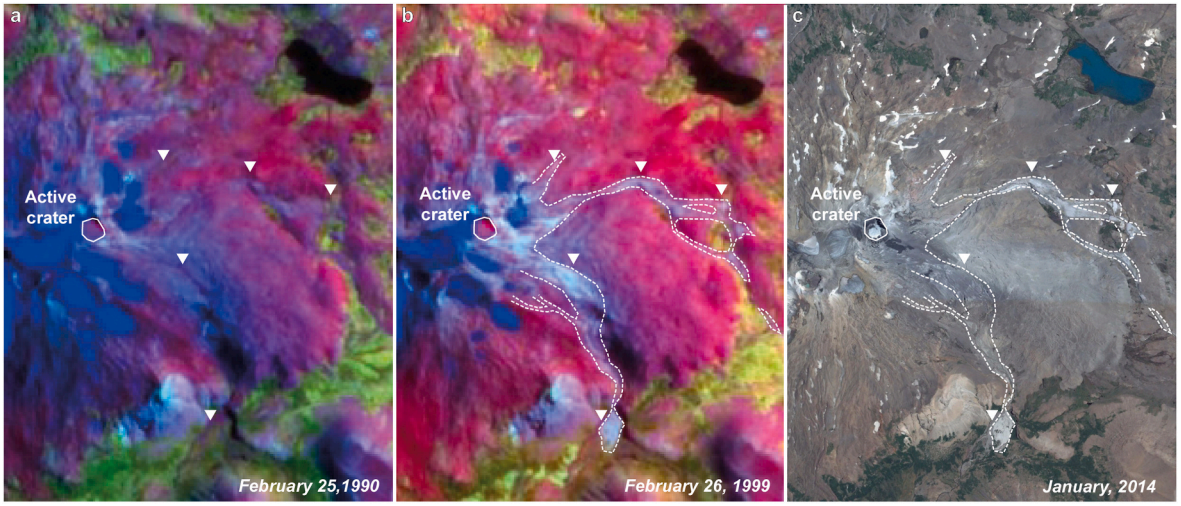

Fig. 8. Comparison of satellite images of the eastern flank of the Copahue volcano taken in different years. Dashed lines indicate the WHD and white triangles are point of comparison. **a.** LandSat 4 TM image acquired on February 25, 1990 (bands combination 653: RGB). **b.** LandSat 5 TM acquired on February 26, 1999 (bands combination 653: RGB). **c.** Google earth images acquired in January 2014.

volcaniclastic lithofacies, these sequences present a subglacial sheet lava with glassy chilled margins, cooling joints characteristic of rapid chilling in presence of water/ice, and maybe locally pillowed (Smellie, 2008; Smellie and Edwards, 2016). This lava is generally encased by a massive or crudely planar stratified hyaloclastite breccia. Finally, the sequences are usually covered by subaerial lavas that can present steep margins due to the interaction with ice walls (Smellie, 2008).

The close relationship, the similar general composition, and the absence of unconformities between the PBD and the upper subglacial lavas/hyaloclastites indicate a cogenetic association and support a similar interpretation of the sheet-like (or esker-like). The soft-sediment deformation present in the deposits indicates a water-saturated setting and supports this interpretation. Following this line, Báez et al. (2020) considered the PBD as a deposit emplaced by these syn-eruptive subglacial meltwater flows and rejecting the interpretation as a wet dilute PDC deposit due to the lack of distinctive features (e.g. impact sag structures, accretionary lapilli, armoured lapilli, or fine ash draping beds). Also, it should be noted that the emplacement of PDCs in subglacial tunnels is unlikely. Broadly similar deposits of fines-poor, cross- and parallel-bedded gravel and sand are common in glacial eskers (Banerjee and McDonald, 1975; Smellie and Skilling, 1994).

During subglacial eruptions, large volumes of meltwater are rapidly generated and can be released away from the vent site through subglacial tunnels, forming in some cases devastating floods called Jökulhlaups (Höskuldsson and Sparks, 1997; Wilson and Head, 2002) (Fig. 6a). Thin impermeable ice or alpine-type glacial is necessary for this efficient drainage of the meltwater (Smellie et al., 2011; Smellie and Edwards, 2016). Traction currents, cohesionless debris flows, and

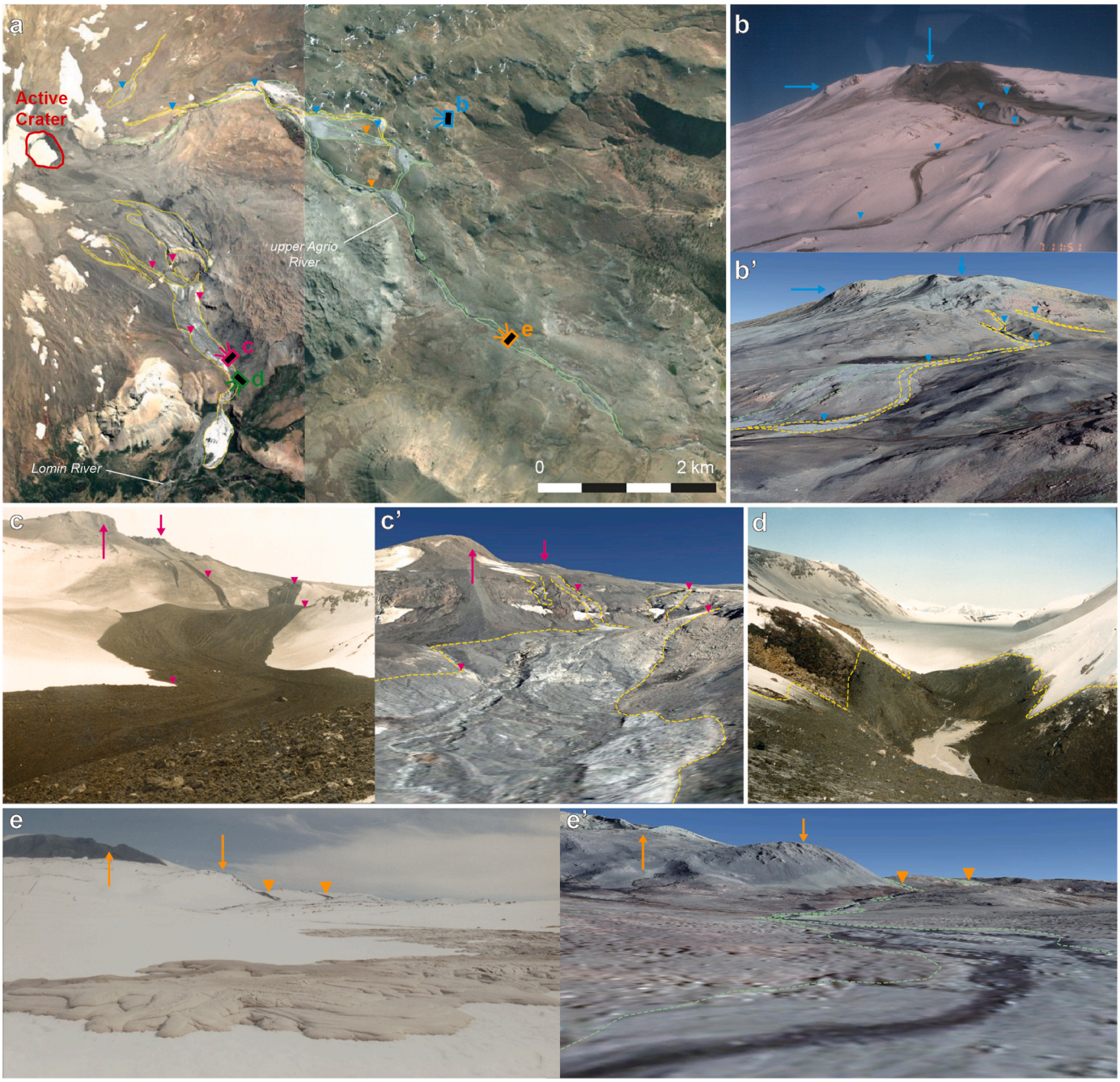

Fig. 9. Comparation between the WHD and the path of the 1992–1995 lahar in the Copahue volcano. **a.** Distribution of the WHD. The different colors of the deposits indicate their possible origin from the 1992 lahar (yellow) or the 1995 lahar (green), interpretated from the description of the eruptions and the photographic evidence. Rectangles indicate the approximate position and direction of the photographs in b, c, d, and e. The triangles indicate the location of the comparison points marked in the following figures. **b.** Lahar generated in the east flank during the 1992 eruption. b'. 3D view of Google Earth image of the same area showing the WHD. **c.** Lahar generated in the southeast flank during the 1992 eruption. c'. 3D view of Google Earth image of the same area showing the WHD. **d.** Deposit of the lahar generated in the southeast flank during the 1992 eruption after the melting of part of the snow cover. In the background is showing the valley of the Lomín river. **e.** Lahar generated in the east flank during the 1995 eruption. Note the formation of frontal lobules and the lack of marginal levees. e'. 3D view of Google Earth image of the same area showing the WHD. Photographs b, c, and d courtesy of Higinio del Monte, and photograph e courtesy of Tony Huglich.

hyperconcentrated flows have been interpreted as the origin of similar volcaniclastic deposits of syn-eruptive meltwater flows (e.g. Smellie and Skilling, 1994; Loughlin, 2002; Smellie, 2008; Bennett et al., 2009). In the case of the PBD, based on the granulometric, textural, and bedding characteristics we propose a deposition mainly from hyperconcentrated flows (McPhie et al., 1993; Benvenuti and Martini, 2002; Pierson, 2005). The generation of these flows represents a common phenomenon in Jökulhlaups (Russell and Knudsen, 2002; Duller et al., 2008; Marren and Schuh, 2009). An initial debris flow that rapidly dilutes and evolves into a hyperconcentrated flow may be represented by the locally preserved basal breccia. The rhythmites composed of inverse graded beds locally present in the PBD are interpreted as deposited from traction carpets (Todd, 1989; Sohn, 1997; Benvenuti and Martini, 2002). Coarse-sand and fine-gravel rhythmites have also been described in Jökulhlaups deposits (Russell and Knudsen, 1999; Russell and Arnott, 2003).

The syn-eruptive subglacial meltwater flows can rework and

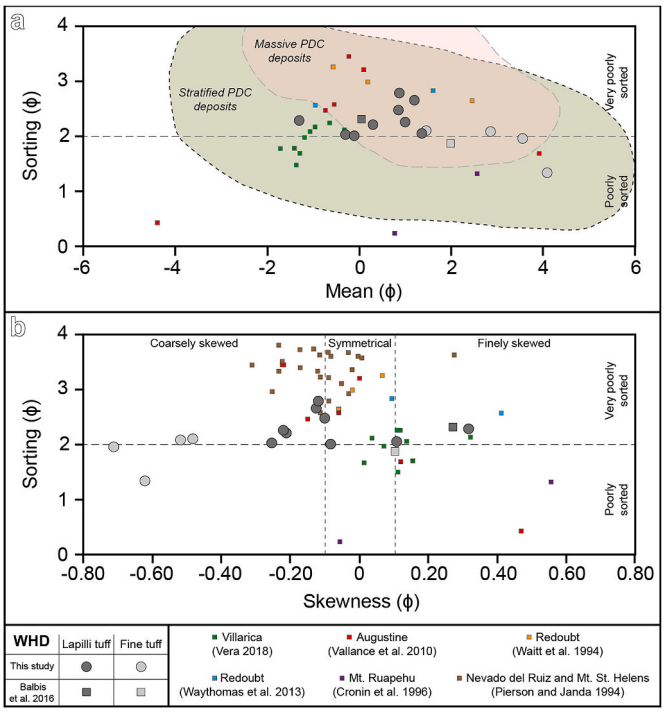

Fig. 10. Granulometric characteristics of the WHD and previously described mixed avalanche deposits for comparison. Reference cited in the figure (The parameters corresponding to Balbis et al., 2016 were calculated from the data presented in that article). **a.** Scatter plot of mean versus sorting. Grainsize distribution of PDC deposits for comparison is from Brown and Andrews (2015). **b.** Scatter plot of skewness versus sorting. Phi scale: $\phi = -\log_2$ (grain diameter in mm).

redeposit two main types of fragments generated in the associated eruption: vesicular vitroclasts formed during explosive phreatomagmatic eruptions, and non-vesicular blocky vitroclasts formed by in situ hyaloclastic fragmentation (Smellie, 2008, 2009; Banik et al., 2014; Lachowycz et al., 2015). The poor to non-vesicularity, the angularity, and the presence of overcooling textures in the fragments present in the PBD indicate a main contribution of hyaloclastic fragments (Fig. 6b). Fragments from explosive eruptions are not present in the PBD, although phreatomagmatic activity in the vent is expected in this context and its occurrence is not refused. Quick and effective drainage in the vent area, added to high effusion rates could explain a poor development of the explosive activity. Also, no pillow fragments were recognized within the deposit, which supports poor ponding of the meltwater and effective drainage. Nevertheless, the presence of isolated sulfur fragments would indicate the formation of a subglacial lake before the eruption, suggesting a vent configuration similar to the currently active crater.

The characteristics of the fractured lavas located above the PBD evidence an interaction with ice/water during the emplacement and reminds those present in the sheet-like sequences. During the formation of these sequences, lava flows emitted from the vent can flow downslope through the subglacial tunnels formed by the meltwater flows (Smellie and Skilling, 1994; Lescinsky and Fink, 2000). This origin is proposed by the thin sheet lavas associated with hyaloclastite breccias emplaced over the PBD (Fig. 6c). The abundant hyaloclastite breccia in the top of the sheet lava evidence the interaction with the ice and the minor basal hyaloclastite breccia would have been formed by the contact with the underlying water-saturated sediments (Smellie and Skilling, 1994). Usually, the thin ice on the tunnel roof is subsequently disintegrated allowing the emplacement of subaerial lithofacies (Smellie, 2008; Smellie and Edwards, 2016). The upper over-thickened jointed lavas are interpreted as ice-confined subaerial lavas emplaced in this context (Fig. 6d).

5.1.3. Distal Holocene Deposits (DHD)

The predominance of fine-size material forming aggregates and the presence of diatoms and high organic content in the DHD, support the interpretation of a sedimentary deposition probably in a lacustrine setting, and refuses the original interpretation as PDC deposits. The contribution of volcanic materials is well evidenced by the presence of glass shards, which may correspond to fallen material or have been transported by tributaries. Since lakes are low-energy environments where sediments accumulate almost continuously, dateable organic matter is present, and tephra can be preserved, they may represent a useful record of volcanic activity (White and Riggs, 2001; De Fontaine et al., 2007). The presence of a massive fabric could indicate the action of pedogenic processes that obliterated original characteristics of the deposit such as lamination.

Considering its location, the DHD would have deposited during a higher paleo-level of the Caviahue lake during the Holocene. The altitude of these deposit coincides with the deposits located to the west of the current coast of the Caviahue lake mapped as lacustrine deposits (Melnick et al., 2006) (Fig. 7). It is a remarkable fact that aggregates with similar characteristics to those present in the DHD and high organic contents have been observed in sediment cores obtained from the current Caviahue lake (Cerrato, 2020).

5.1.4. Whitish Historic Deposit (WHD)

Different possible ages have been proposed for this deposit regardless of its genetic interpretation: 1961 (Petrinovic et al., 2014a), 1992–1995 (Delpino and Bermúdez, 1993; Bermúdez and Delpino, 1995; Polanco, 2003; Sruoga and Consoli, 2011a), and 2000 (Balbis et al., 2016). To solve this discrepancy, we analyzed a LandSat 4 TM image acquired on February 25, 1990, and a LandSat 5 TM acquired on February 26, 1999 (Fig. 8). The absence of the WHD in the 1990 image and the presence in the 1999 image limit the possible temporal range of its formation. Therefore, considering the recent eruptive history of the Copahue volcano, the WHD would have been deposited during the 1992–1995 eruptions.

The similar components and distribution between the WHD and the 1992 and 1995 lahars, added to the age range obtained, support the interpretation of the WHD as a lahar deposit (Fig. 9). The main evidence to reject this interpretation is the assertion that the lithofacial characteristics observed in this deposit cannot be explained by lahar processes (Balbis et al., 2016). However, the characteristics of the WHD are similar to those observed in volcanic mixed avalanche deposits (also called ice-rich lahars or ice-slurries lahars). Although these processes are not mentioned by this name for the 1992–1995 eruptions, the ice-bearing lahars described by Delpino and Bermúdez (1993) could correspond to these, indicating only a nomenclature problem.

A volcanic mixed avalanche is defined as a flow composed of a mixture of snow/ice, water, and tephra in which the solid particles are partially supported by the snow/ice fraction (Vallance et al., 2010). This process has been observed in several snow/ice-clad volcanoes, however, there are not many detailed descriptions of its deposits (e.g. Cronin et al., 1996; Kilgour et al., 2010; Vallance et al., 2010; Waythomas et al., 2013; Romero et al., 2018), even less after the melting of the snow/ice fraction (e.g. Pierson and Janda, 1994; Waitt et al., 1994; Lube et al., 2009; Breard et al., 2020). Post melting deposits consist of poorly compacted thinner massive layers with no obvious characteristics of typic lahars and low potential for preservation and recognition in the geologic record (Pierson and Janda, 1994; Lube et al., 2009; Waythomas, 2014).

The solid fraction in mixed avalanche deposits is poorly sorted and present a predominance of ash-size clasts, followed by lapilli-size (even block-size), and a small proportion of clasts smaller than, showing weakly negatively skewed bimodal to polymodal grain-size distribution (Pierson and Janda, 1994; Lube et al., 2009; Breard et al., 2020). However, Waitt et al. (1994) mention < 62 μm-thick clast fractions between 8% and 24%. These granulometric characteristics are similar to

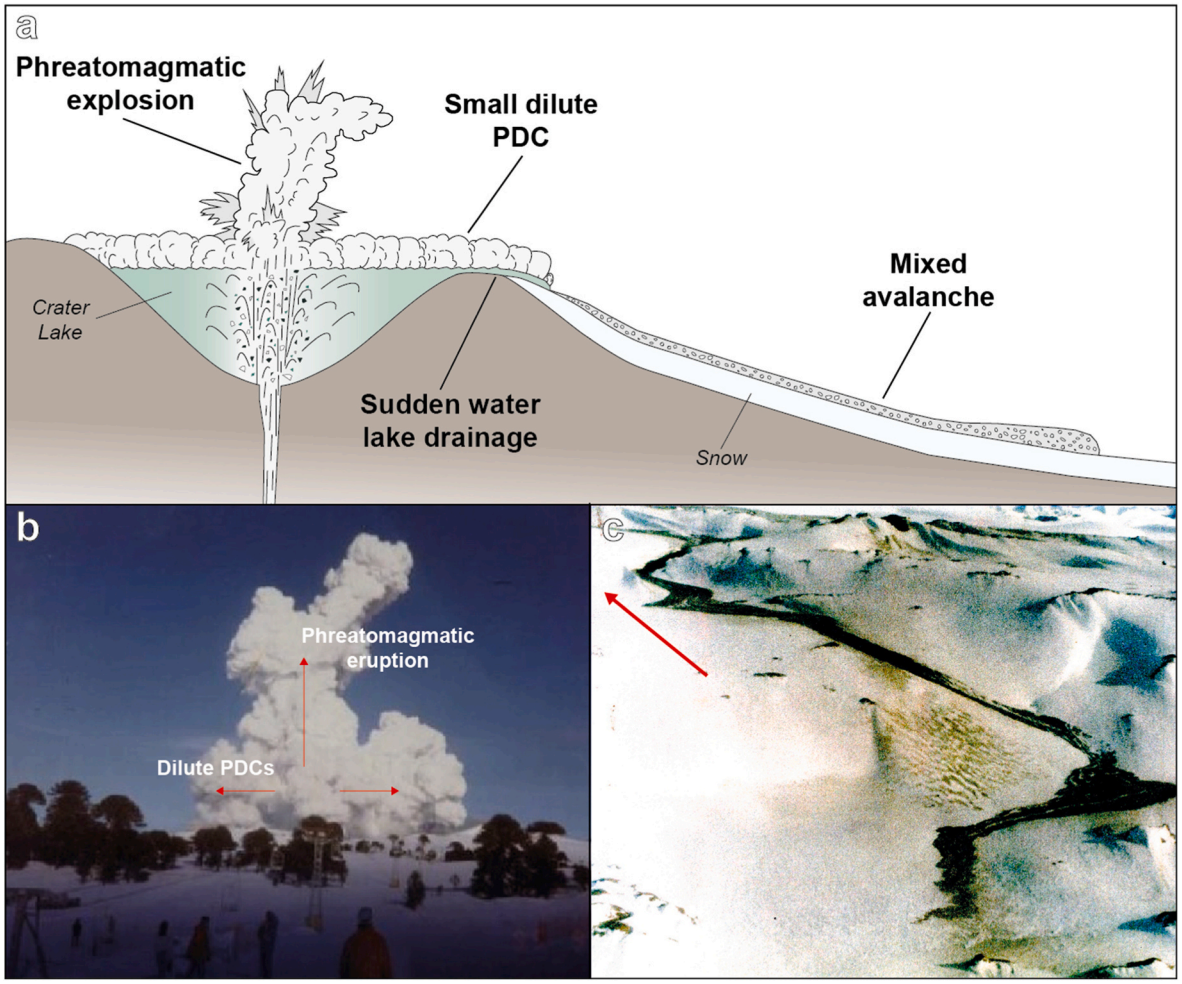

Fig. 11. Genesis of the forming-WHD mixed avalanche. **a.** Schematic illustration of the possible genesis of the mixed avalanche during a phreatomagmatic eruption in the crater lake. The effect of the dilute PDCs, or the lake water expelled from the lake, on the snow present on the flank of the edifice triggers the mixed avalanche. **b**. Photograph of the 1995 eruption of the Copahue volcano to exemplify the model of mixed-avalanche formation (modified from Caselli et al., 2016a). **c.** The 1992 lahar (mixed avalanche) flowing over the snow cover (Photograph courtesy of Higinio del Monte). The red arrow indicates the location of the active crater.

those observed in the lapilli tuff lithofacies of the WHD (Fig. 10). It should be noted that these characteristics are also expected in PDC deposits, so, in this case, the granulometric information is ambiguous and, by itself, it does not allow the determination of the origin of the deposit. The samples of fine tuff lithofacies analyzed in this study present extreme values in some granulometric parameters, probably due to methodological problems in the sieving, so these values should be considered with caution.

Pierson and Janda (1994) describe in some mixed avalanche deposits the presence of fine-grained basal layers probably equivalent to the sole layers of the debris-flows, which could explain the formation of the fine tuff lithofacies. Lube et al. (2009) also mention centimetric fine-rich drapes in deposits after melting, but not associated with basal positions. Breard et al. (2020) describe a mixed avalanche deposit with inverse grading at the top, similarly to the WHD, although they also mention a weak normal grading at the bottom.

The preservation of the WHD adhered to the bends of channels also has been used as criteria to its interpretation as PDC deposit (Balbis et al., 2016). However, superelevation has also been observed in the bends of mixed avalanches, with preservation of the deposit on the outside of the channel bends (Cronin et al., 1996; Kilgour et al., 2010). It is important to note that the maximum height reached by the WHD may be considerably overestimated due to the unawareness of the original flow thickness considering the topographic smoothing effect caused by the significant snow cover. The lack of levees and the generation of marginal lobes present in the WHD is described in several mixed avalanches (e.g. Vallance et al., 2010; Breard et al., 2020), although in some cases marginal levees were mentioned (e.g. Kilgour et al., 2010).

Lastly, the mentions of charred bushes in the WHD (Petrinovic et al., 2014a; Balbis et al., 2016) is evidence of high temperatures during its emplacement, which are not expected in mixed avalanches. The presence of these charred bushes could not be verified by our field observations. Considering the partial charring condition of the mentioned bushes and the lack of other evidence of high temperature like thermal oxidation of clasts, a more detailed analysis is required to constrain a possible temperature range. An interesting fact to take into account is the presence of a significant snow cover during the eruptions that would have protected the vegetation (e.g. Vallance et al., 2010).

Although the granulometric information can be ambiguous, based on the possible age range and the general distribution and architecture of the WHD, and considering the description of the eruptive activity during this period, we interpret that the most feasible origin for the WHD is from mixed avalanches generated during the 1992–1995 eruptive activity of the Copahue volcano (Fig. 11a). This origin coincides with the original interpretation of the WHD as ice-bearing lahars (Delpino and Bermúdez, 1993; Bermúdez and Delpino, 1995). The mixed avalanches would have been triggered during phreatomagmatic eruptions by the effect of dilute PDCs, or the water expelled from the lake, on the snow (Fig. 11b). These flowed over the snow/ice cover reaching great distances from the crater due to its high mobility (e.g. Lube et al., 2009;

Breard et al., 2020) (Fig. 11c).

5.2. Evidence of PDCs and hazards implications

As discussed in the previous sections, the four analyzed deposits previously interpreted as PDC products, would not have this origin. This reflects a previous overestimation of the occurrence of major PDCs in the evolution of the Copahue volcano. Similarly, Hernando et al. (2020) also reinterpret a clastic deposit from previous stages of the Caviahue-Copahue Volcanic Complex that was originally considered a PDC deposit, as being deposited within a deltaic to alluvial system.

The correct interpretation and mapping of the deposits associated with a volcano can indicate the age, style, volume, and distribution of past eruptions. Thus, allowing forecasting the possible characteristics of future eruptions and consequently, these play a fundamental role in the hazard mapping and assessment (Tilling, 2008). The first hazard map of the Copahue volcano (Bermúdez and Delpino, 1995) considers only the Argentine sector and establishes an area of 5 km around the active crater as susceptible of being affected by dilute PDCs during phreatomagmatic eruptions. The most recent hazard map (Naranjo et al., 2000) considers the pyroclastic deposits interpreted by Polanco (1998) and establishes the entire Caviahue Caldera as a zone with very low potential to be affected by PDCs. The new evidence presented in this contribution should be considered in the elaboration of new hazard maps.

Considering the evidence presented here and the descriptions of historical eruptions (Naranjo and Polanco, 2004; Petrinovic et al., 2014b; Caselli et al., 2016b), the area potentially affected by PDCs in the Copahue volcano would be limited near the active crater, without representing a risk in themselves for the Caviahue and Copahue towns. In this context, the generation of large PDCs is unlikely, although the possibility of their occurrence in the future cannot be completely ruled out.

Considering the crater lake, the glacier located in the summit, and the significant winter snow cover, the generation of flows due to the melting of snow/ice during volcanic activity and the sudden drainage of the crater lake, even during a lake break-out lahar, appear to be more likely a potential hazard capable of affecting large areas. However, a detailed analysis that includes the modeling of the processes that could potentially occur in the Copahue volcano is necessary to make more concrete assertions.

6. Conclusions

Four key deposits previously interpreted as PDCs products corresponding to different stages of the Copahue volcano evolution (Pleistocene, Holocene, and Historic times) have been analyzed and their origin discussed:

- The reddish succession located in the northeast flank (NRS) is considered as a succession of clastogenic lavas, following the interpretation proposed by Báez et al. (2020).
- The proximal bedded volcaniclastic deposits (PBD) are considered as redeposition of hyaloclastic fragments from syn-eruptive subglacial meltwater flows. The association of the PBD with subglacial lavas and hyaloclastites supports the interpretation of a like sheet-like sequence or esker-like sequence.
- The distal Holocene deposit located north of Lake Caviahue (DHD) are reinterpreted as sedimentary (lacustrine) deposits with the input of volcaniclastic material.
- The historic whitish-grey clastic deposit located on the eastern flank (WHD) is interpreted as product of mixed avalanches generated during the 1992–1995 activity, according to its original interpretation (Delpino and Bermúdez, 1993; Bermúdez and Delpino, 1995).

The evidence presented here indicates that the PDCs occurrence during the Copahue volcano evolution is less than previously thought. Large PDCs are unlikely in the future and their influence area would be reduced near the active crater as observed in recent eruptions. Flows triggered by the melting of snow/ice during volcanic activity and sudden drainage of the crater lake appear to be a more likely potential hazard that should be considered during risk assessment.

Declaration of competing interest

The authors declare that they have no known competing financial interests or personal relationships that could have appeared to influence the work reported in this paper.

Acknowledgements

This work was supported by Universidad Nacional de Río Negro (project PI UNRN 2019 40 A 795). We thanks to the *Departamento de Caracterización de Materiales* (*Centro Atómico Bariloche*, Argentina) for their support in XRD studies and access to SEM. We also acknowledge Andres Folguera for editorial handling, and Guido Giordano and an anonymous reviewer for their helpful comments that have substantially improved this paper.

Appendix A. Supplementary data

Supplementary data to this article can be found online at https://doi.org/10.1016/j.jsames.2021.103479.

Author statement

Alejandro D. Báez: Writing – original draft, Visualization, Project administration; Walter Báez: Writing – original draft, Visualization, Supervision; Alberto T. Caselli: Writing – review & editing; Funding acquisition, Supervision; Romina Daga: Writing – review & editing; Carlos A. Sommer: Writing – review & editing.

References

Agusto, M., Varekamp, J., 2016. The Copahue Volcanic-Hydrothermal System and applications for volcanic surveillance. In: Tassi, F., Vaselli, O., Caselli, A.T. (Eds.), Copahue Volcano, Active Volcanoes of the World. Springer, Berlin, Heidelberg, pp. 49–59. https://doi.org/10.1007/978-3-662-48005-2_9.

Andronico, D., Cristaldi, A., Scollo, S., 2008. The 4–5 september 2007 lava fountain at south-east crater of Mt etna, Italy. J. Volcanol. Geoth. Res. 173, 325–328. https://doi:10.1016/j.jvolgeores.2008.02.004.

Auker, M.R., Sparks, R.S.J., Siebert, L., Crosweller, H.S., Ewert, J., 2013. A statistical analysis of the global historical volcanic fatalities record. J Appl. Volcanol. 2, 2. https://doi.org/10.1186/2191-5040-2-2.

Báez, A.D., Báez, W., Caselli, A.T., Martini, M., Sommer, C.A., 2020. The glaciovolcanic evolution of the Copahue volcano, andean southern volcanic zone, Argentina-Chile. J. Volcanol. Geoth. Res. 396, 106866. https://doi.org/10.1016/j.jvolgeores.2020.106866.

Balbis, C., Petrinovic, I.A., Guzmán, S., 2016. A contribution to the hazards assessment at Copahue volcano (Argentina-Chile) by facies analysis of a recent pyroclastic density current deposit. J. Volcanol. Geoth. Res. 327, 288–298. https://doi.org/10.1016/j.jvolgeores.2016.08.009.

Banerjee, I., McDonald, B.C., 1975. Nature of esker sedimentation. In: Jopling, A.V., McDonald, B.C. (Eds.), Glaciofluvial and Glaciolacustrine Sedimentation. Society of Economic Paleontologist and Mineralogists, Spl. Pub. No. 23, pp. 132–154.

Banik, T.J., Wallace, P.J., Höskuldsson, Á., Miller, C.F., Bacon, C.R., Furbish, D.J., 2014. Magma–ice–sediment interactions and the origin of lava/hyaloclastite sequences in the Sída Formation, South Iceland. Bull. Volcanol. 76, 785–803. https://doi.org/10.1007/s00445-013-0785-3.

Bennett, M.R., Huddart, D., Gonzalez, S., 2009. Glaciovolcanic landsystem and largescale glaciotectonic deformation along the Brekknafjöll–Jarlhettur, Iceland. Quat. Sci. Rev. 28, 647–676. https://doi.org/10.1016/j.quascirev.2008.07.018.

Benvenuti, M., Martini, I.P., 2002. Analysis of terrestrial hyperconcentrated flows and their deposits. Spec. Publs int. Ass. Sediment. 32, 167–193. https://doi.org/10.1002/9781444304299.ch10.

Bermúdez, A., Delpino, D., 1995. Mapa de los peligros potenciales en el área del Volcán Copahue Sector Argentino. Serie Mapas de Riesgo Geológico. Servicio Geológico Neuquino, Neuquén.

Blott, S.J., Pye, K., 2001. GRADISTAT: a grain size distribution and statistics package for the analysis of unconsolidated sediments. Earth Surf. Process. Landforms 26 (11), 1237–1248. https://doi.org/10.1002/esp.261.

Branney, M.J., Kokelaar, P., 2002. Pyroclastic Density Currents and the Sedimentation of Ignimbrites. Geol. Soc., London, United Kingdom.
Breard, E.C.P., Calder, E.S., Ruth, D.C.S., 2020. The interaction between concentrated pyroclastic density currents and snow: a case study from the 2008 mixed-avalanche from Volcán Llaima (Chile). Bull. Volcanol. 82, 75.
Brown, R.J., Blake, S., Thordarson, T., Self, S., 2014. Pyroclastic edifices record vigorous lava fountains during the emplacement of a flood basalt flow field, Roza Member, Columbia River Basalt Province, USA. GSA Bulletin 126 (7–8), 875–891. https://doi.org/10.1130/B30857.1.
Brown, R.J., Andrews, G.D., 2015. Deposits of pyroclastic density currents. In: Sigurdsson, H., Houghton, B., McNutt, S., Rymer, H., Stix, J. (Eds.), Encyclopedia of Volcanoes, second ed. Academic Press, pp. 631–648. https://doi.org/10.1016/B978-0-12-385938-9.00036-5.
Carracedo Sánchez, M., Sarrionandia, F., Arostegui, J., Eguiluz, L., Gil Ibarguchi, J.I., 2012. The transition of spatter to lava-like body in lava fountain deposits: features and examples from the Cabezo Segura volcano (Calatrava, Spain). J. Volcanol. Geoth. Res. 227–228, 1–14. https://doi.org/10.1016/j.jvolgeores.2012.02.016.
Cas, R.A.F., Wright, J.V., 1987. Volcanic Successions: Modern and Ancient. Allen & Unwin, London, p. 528. https://doi.org/10.1007/978-94-009-3167-1.
Caselli, A.T., Velez, M.L., Agusto, M., Liccioli, C., Vaselli, O., 2016a. Prehistoric to historic volcanic activity at Copahue Volcano. In: Tassi, F., Vaselli, O., Caselli, A.T. (Eds.), Copahue Volcano, Active Volcanoes of the World. Springer, Berlin, Heidelberg, pp. 49–59. https://doi.org/10.1007/978-3-662-48005-2_3.
Caselli, A.T., Agusto, M., Velez, M.L., Forte, P., Bengoa, C., Daga, R., Albite, J.M., Capaccioni, B., 2016b. The 2012 eruption. In: Tassi, F., Vaselli, O., Caselli, A.T. (Eds.), Copahue Volcano, Active Volcanoes of the World. Springer, Berlin, Heidelberg, pp. 61–77. https://doi.org/10.1007/978-3-662-48005-2_4.
Caselli, A.T., Sommer, C.A., Daga, R., Báez, A.D., Barion, G.E., 2018. Volcán Copahue: Fases eruptivas del ciclo 2012-2018. XV Congreso Geológico Chileno, Concepción, Chile, p. 1064.
Cashman, K.V., Scheu, B., 2015. Magmatic fragmentation. In: Sigurdsson, H., Houghton, B., McNutt, S., Rymer, H., Stix, J. (Eds.), Encyclopedia of Volcanoes, second ed. Academic Press, pp. 459–471. https://doi.org/10.1016/B978-0-12-385938-9.00025-0.
Cassidy, M., Manga, M., Cashman, K., Bachmann, O., 2018. Controls on explosive-effusive volcanic eruption styles. Nat. Commun. 9, 2839. https://doi.org/10.1038/s41467-018-05293-3.
Cerrato, J., 2020. Variación mineralógica de una secuencia sedimentaria lacustre de un ambiente ácido natural con influencia volcánica: Lago Caviahue (37,8°S 71°O), Norpatagonia, Argentina. Thesis, Universidad Nacional del Comahue.
Cole, R.P., White, J.D.L., Conway, C.E., Leonard, G.S., Townsend, D.B., Pure, L.R., 2018. The glaciovolcanic evolution of an andesitic edifice, south crater, Tongariro volcano, New Zealand. J. Volcanol. Geoth. Res. 352, 55–77. https://doi.org/10.1016/j.jvolgeores.2017.12.003.
Cronin, S.J., Neall, V.E., Jérome, A.L., Palmer, A.S., 1996. Unusual "snow slurry" lahars from Ruapehu volcano, New Zealand, September 1995. Geology 24 (12), 1107–1110.
Daga, R., Caselli, A.T., Ribeiro Guevara, S., Agusto, M., 2017. Tefras emitidas durante la fase inicial hidromagmática (julio de 2012) del ciclo eruptivo 2012-actual (2016) del volcán copahue (andes del sur). Rev. Asoc. Geol. Argent. 74 (2), 191–206.
De Fontaine, C., Kaufman, D., Scott Anderson, R., Werner, A., Waythomas, C., Brown, T., 2007. Late Quaternary distal tephra-fall deposits in lacustrine sediments, Kenai Peninsula, Alaska. Quat. Res. 68 (1), 64–78. https://doi.org/10.1016/j.yqres.2007.03.006.
Delpino, D., Bermúdez, A., 1993. La actividad del Volcán Copahue durante 1992. Erupción con emisiones de azufre piroclástico. In: Provincia del Neuquén – Argentina, vol. 4. XII Congreso Geológico Argentino, Mendoza, Argentina, pp. 292–301.
Delpino, D., Bermúdez, A., 1994. Volcanismo post-glacial en el volcan Copahue (37°45'S) sector argentino. Peligros potenciales asociados. VII Congreso Geológico Chileno, Puerto Varas, Chile 1, 260–264.
Delpino, D., Bermúdez, A., 2002. La erupción del volcán Copahue del año 2000. Impacto social y al medio natural. Provincia del Neuquén. Argentina. XV Congreso Geológico Argentino 3, 365–370.
Duller, R.A., Mountney, N.P., Russell, A.J., Cassidy, N.C., 2008. Architectural analysis of a volcaniclastic jökulhlaup deposit, southern Iceland: sedimentary evidence for supercritical flow. Sedimentology 55, 939–964. https://doi.org/10.1111/j.1365-3091.2007.00931.x.
Edwards, B.R., Russell, J.K., 2002. Glacial influences on morphology and eruptive products of Hoodoo Mountain volcano, Canada. In: Smellie, J.L., Chapman, M.G. (Eds.), Volcano–ice Interaction on Earth and Mars, vol. 202. Geol. Soc. Spec. Pub., London, pp. 179–194.
Folk, R.L., Ward, W.C., 1957. Brazos River bar: a study in the significance of grain size parameters. J. Sediment. Petrol. 27, 3–26.
Forte, P.B., Caselli, A.T., 2014. Nuevas evidencias de actividad explosiva en el volcán Copahue durante el periodo preglaciario. In: Andes del Sur – Argentina, S23. XIX Congreso Geológico Argentino, Córdoba, Argentina, p. 18.
Frontoni, A., Vona, A., Giordano, G., Viccaro, M., Romano, C., 2019. The emplacement of a clastogenic lava flow: a rheological perspective. Geophys. Res. Abstr. 21, 1.
GVP (Global Volcanism Program), 1992. Report on copahue (Chile-Argentina). Bull. Glob. Volcanism Netw. 17, 7 (Smithsonian Institution).
GVP (Global Volcanism Program), 2013. Copahue (357090). In: Venzke, E. (Ed.), Volcanoes of the World, V. 4.9.0 (04 Jun 2020). Smithsonian Institution. https://doi.org/10.5479/si.GVP.VOTW4-2013. Downloaded 11 Sep. 2020.
Heiri, O., Lotter, A.F., Lemcke, G., 2001. Loss on ignition as a method for estimating organic and carbonate content in sediments: reproducibility and comparability of results. J. Paleolimnol. 25 (1), 101–110.
Hernando, I.R., Bucher, J., del Papa, C.E., Eisermann, J.O., Göllner, P.L., Guzmán, S.R., Balbis, C., Petrinovic, I.A., 2020. Unraveling the timing of the Caviahue depression, andean southern volcanic zone: insights from the sedimentary infill. Int. J. Earth Sci. https://doi.org/10.1007/s00531-020-01936-3.
Höskuldsson, A., Sparks, R.S.J., 1997. Thermodynamics and fluid dynamics of effusive subglacial eruptions. Bull. Volcanol. 59, 219–230.
Houghton, B., 2015. Explosive volcanism. In: Sigurdsson, H., Houghton, B., McNutt, S., Rymer, H., Stix, J. (Eds.), Encyclopedia of Volcanoes, second ed. Academic Press, pp. 457–458. https://doi.org/10.1016/B978-0-12-385938-9.02006-X.
Houghton, B., White, J.D.L., Van Eaton, A.R., 2015. Phreatomagmatic and related eruption styles. In: Sigurdsson, H., Houghton, B., McNutt, S., Rymer, H., Stix, J. (Eds.), Encyclopedia of Volcanoes, second ed. Academic Press, pp. 537–552. https://doi.org/10.1016/B978-0-12-385938-9.00030-4.
Kilgour, G., Manville, V., Della Pasqua, F., Graettinger, A., Hodgson, K.A., Jolly, G.E., 2010. The 25 September 2007 eruption of Mount Ruapehu, New Zealand: directed ballistics, surtseyan jets, and ice-slurry lahars. J. Volcanol. Geoth. Res. 191, 1–14. https://doi.org/10.1016/j.jvolgeores.2009.10.015.
Lachowycz, S.M., Pyle, D.M., Gilbert, J.S., Mather, T.A., Mee, K., Naranjo, J.A., Hobbs, L.K., 2015. Glaciovolcanism at Volcán Sollipulli, southern Chile: lithofacies analysis and interpretation. J. Volcanol. Geoth. Res. 303, 59–78. https://doi.org/10.1016/j.jvolgeores.2015.06.021.
Lescinsky, D.T., Fink, J.H., 2000. Lava and ice interaction at stratovolcanoes: use of characteristic features to determine past glacial extents and future volcanic hazards. J. Geophys. Res. 105, 23711–23726. https://doi.org/10.1029/2000JB900214.
Linares, E., Ostera, H.A., Mas, L., 1999. Cronología Potasio-Argón del complejo efusivo Copahue-Caviahue, Provincia de Neuquén. Rev. Asoc. Geol. Argent. 54 (3), 240–247.
Loughlin, S.C., 2002. Facies analysis of proximal subglacial and proglacial volcaniclastic successions at the Eyjafjallajökull central volcano, southern Iceland. In: Smellie, J.L., Chapman, M.G. (Eds.), Volcano–ice Interaction on Earth and Mars, vol. 202. Geol. Soc. Spec. Pub., London, pp. 149–178. https://doi.org/10.1144/GSL.SP.2002.202.01.08.
Lube, G., Cronin, S.J., Procter, J.N., 2009. Explaining the extreme mobility of volcanic ice-slurry flows, Ruapehu volcano, New Zealand. Geology 37 (1), 15–18. https://doi.org/10.1130/G25352A.1.
Maro, G., Caffe, P.J., 2016. Neogene monogenetic volcanism from the Northern Puna region: products and eruptive styles. In: Németh, K., Carrasco-Núñez, G., Aranda-Gómez, J.J., Smith, I.E.M. (Eds.), Monogenetic Volcanism. Geological Society, London, Special Publications, pp. 337–360.
Marren, P.M., Schuh, M., 2009. Criteria for identifying jökulhlaup deposits in the sedimentary record. In: Burr, D.M., Carling, P.A., Baker, V.R. (Eds.), Megaflooding on Earth and Mars. Cambridge University Press, pp. 225–242.
McPhie, J., Doyle, M., Allen, R., 1993. Volcanic Textures: a Guide to the Interpretation of Textures in Volcanic Rocks. CODES Key Centre, University of Tasmania, Hobart, p. 196.
Melnick, D., Folguera, A., Ramos, V.A., 2006. Structural control on arc volcanism: the Copahue-Agrio complex, South-Central Andes (37°50′S). J. S. Am. Earth Sci. 22, 66–88. https://doi.org/10.1016/j.jsames.2006.08.008.
Moorhouse, B.L., White, J.D.L., 2016. Interpreting ambiguous bedforms to distinguish subaerial base surge from subaqueous density current deposits. Depos. Rec. 2, 173–195. https://doi.org/10.1002/dep2.20.
Naranjo, J.A., Moreno, H., Polanco, E., Young, S., 2000. Mapa de peligros de los volcanes del Alto Biobio. Regiones del BioBio y de la Araucanía. Documento de trabajo N °15. Servicio Nacional de Geología y Minería de Chile.
Naranjo, J.A., Polanco, E., 2004. The 2000 AD eruption of Copahue volcano, southern andes. Rev. Geol. Chile 31, 279–292.
Petit-Breuilh, M.E., 2004. La historia eruptiva de los volcanes hispanoamericanos (siglos XVI al XX): el modelo chileno. Servicio de Publicaciones, Cabildo Insular de Lanzarote, Huelva, p. 431.
Petrinovic, I.A., D'Elia, L., Páez, G., Balbis, C., Guzmán, S., Villarosa, G., Carniel, R., 2014a. Depósito de corriente piroclástica reciente (1963-64 AD? - 1976 AD?) del volcán Copahue (I): evidencias geológicas de campo y edad radiocarbónica. Rev. Asoc. Geol. Argent. 71 (1), 139–142.
Petrinovic, I.A., Villarosa, G., D'Elia, L., Guzmán, S.P., Páez, G.N., Outes, V., Manzoni, C., Delménico, A., Balbis, C., Carniel, R., Hernando, I.R., 2014b. La erupción del 22 de diciembre de 2012 del volcán Copahue, Neuquén, Argentina: caracterización del ciclo eruptivo y sus productos. Rev. Asoc. Geol. Argent. 71 (2), 161–173.
Pierson, T.C., 2005. Hyperconcentrated flow – transitional process between water flow and debris flow. In: Jakob, M., Hungr, O. (Eds.), Debris-flow Hazards and Related Phenomena. Springer, Berlin, Heidelberg, pp. 159–202.
Pierson, T., Janda, R., 1994. Volcanic mixed avalanches: a distinc eruption-triggered mass-flow process at snow-clad volcanoes. Geol. Soc. Am. Bull. 106, 1351–1358.
Polanco, E., 1998. Volcanismo explosivo postglacial en la cuenca del Alto Biobio, Andes del Sur (37°45'-38°30'). Thesis, Universidad de Chile.
Polanco, E., 2003. Evolución del volcán Copahue (37° 45 S) Andes del Sur. M.S. Ph.D. Thesis. Universidad Autónoma de México, México D.F.
Polanco, E., Naranjo, J.A., Young, S., Moreno, H., 2000. Volcanismo Explosivo Holoceno en la Cuenca del Alto Biobío, Andes del Sur (37°45'-38°30'S). IX Congreso Geológico Chileno, Puerto Varas, Actas 2, 59–61.
Riggs, N.R., Duffield, W.A., 2008. Record of complex scoria cone eruptive activity at Red Mountain, Arizona, USA, and implications for monogenetic mafic volcanoes. J. Volcanol. Geoth. Res. 178, 763–776. https://doi.org/10.1016/j.jvolgeores.2015.06.021.

Romero, J.E., Vera, F., Polacci, M., Morgavi, D., Arzilli, F., Alam, M.A., Bustillos, J.E., Guevara, A., Johnson, J.B., Palma, J.L., Burton, M., Cuenca, E., Keller, W., 2018. Tephra from the 3 march 2015 sustained column related to explosive lava fountain activity at volcán villarrica (Chile). Front. Earth Sci. 6, 98. https://doi.org/10.3389/feart.2018.00098.

Russell, H.A.J., Arnott, R.W.C., 2003. Hydraulic-jump and hyperconcentrated-flow deposits of a glacigenic subaqueous fan: oak Ridges moraine, Southern Ontario, Canada. J. Sediment. Res. 73 (6), 887–905.

Russell, A.J., Knudsen, O., 1999. An ice-contact rhythmite (turbidite) succession deposited during the November 1996 catastrophic outburst flood (jökulhlaup), Skeiðarárjökull, Iceland. Sediment. Geol. 127, 1–10.

Russell, A.J., Knudsen, O., 2002. The effects of glacier-outburst flood flow dynamics on ice-contact deposits: november 1996 jökulhlaup, Skeiiarársandur, Iceland. In: Martini, I.P., Baker, V.R., Garzón, G. (Eds.), Flood and Megaflood Processes and Deposits: Recent and Ancient Examples. Spec. Publs Int. Ass. Sediment, vol. 32, pp. 67–83.

Smellie, J.L., 2008. Basaltic subglacial sheet-like sequences: evidence for two types with different implications for the inferred thickness of associated ice. Earth Sci. Rev. 88, 60–80. https://doi.org/10.1016/j.earscirev.2008.01.004.

Smellie, J.L., 2009. Terrestrial subice volcanism: landform morphology, sequence characteristics, environmental influences, and implications for candidate Mars examples. In: Chapman, M.G., Keszthelyi, L.P. (Eds.), Preservation of Random Megascale Events on Mars and Earth: Influence on Geologic History, vol. 453. Geological Society of America Special Paper, pp. 55–76. https://doi.org/10.1130/2009.453(05.

Smellie, J.L., 2013. Quaternary volcanism: subglacial landform. In: Elias, S.A. (Ed.), Encyclopedia of Quaternary Science, second ed., pp. 780–802. https://doi.org/10.1016/B978-0-444-53643-3.00074-1.

Smellie, J.L., Edwards, B.R., 2016. Glaciovolcanism on Earth and Mars: Products, Processes, and Paleoenvironmental Significance. Cambridge University Press, United Kingdom, p. 490. https://doi.org/10.1017/S0954102018000214.

Smellie, J.L., Skilling, I.P., 1994. Products of subglacial volcanic eruptions under different ice thicknesses: two examples from Antarctica. Sediment. Geol. 91, 115–129. https://doi.org/10.1016/0037-0738(94)90125-2.

Smellie, J.L., Rocchi, S., Gemelli, M., Di Vincenzo, G., Armienti, P., 2011. A thin predominantly cold-based Late Miocene East Antarctic ice sheet inferred from glaciovolcanic sequences in northern Victoria Land, Antarctica. Palaeogeogr. Palaeoclimatol. Palaeoecol. 307, 129–149. https://doi.org/10.1016/j.palaeo.2011.05.008.

Sohn, Y.K., 1997. On traction-carpet sedimentation. J. Sediment. Res. 67 (3), 502–509.

Sruoga, P., Consoli, V., 2011. El volcán copahue. In: Leanza, H.A., Arregui, C., Carbone, O., Danieli, J.C., Vallés, J.M. (Eds.), Relatorio del XVIII Congreso Geológico Argentino. Asociación Geológica Argentina, Neuquén, pp. 613–620.

Sulpizio, R., Dellino, P., Doronzo, D.M., Sarocchi, D., 2014. Pyroclastic density currents: state of the art and perspectives. J. Volcanol. Geoth. Res. 283, 36–65. https://doi.org/10.1016/j.jvolgeores.2014.06.014.

Sumner, J.M., 1998. Formation of clastogenic lava flows during fissure eruption and scoria cone collapse: the 1986 eruption of Izu-Oshima Volcano, eastern Japan. Bull. Volcanol. 60, 195–212.

Sumner, J.M., Blake, S., Matela, R.L., Wolff, J.A., 2005. Spatter. J. Volcanol. Geotherm. Res. 142, 49–65.

Taddeucci, J., Edmonds, M., Houghton, B., James, M.R., Vergniolle, S., 2015. Hawaiian and strombolian eruptions. In: Sigurdsson, H., Houghton, B., McNutt, S., Rymer, H., Stix, J. (Eds.), Encyclopedia of Volcanoes, second ed. Academic Press, pp. 485–503. https://doi.org/10.1016/B978-0-12-385938-9.00027-4.

Tilling, R.I., 2008. The critical role of volcano monitoring in risk reduction. Adv. Geosci. 14, 3–11.

Todd, S.P., 1989. Stream-driven, high-density gravelly traction carpets: possible deposits in the Trabeg Conglomerate Formation, SW Ireland and some theoretical considerations of their origin. Sedimentology 36, 513–530.

Vallance, J.W., Bull, K.F., Coombs, M.L., 2010. Pyroclastic flows, lahars, and mixed avalanches generated during the 2006 eruption of augustine volcano. In: Power, J. A., Coombs, M.L., Freymueller, J.T. (Eds.), The 2006 Eruption of Augustine Volcano, Alaska. U.S. Geological Survey Professional Paper 1769, pp. 220–267.

Varekamp, J.C., Ouimette, A.P., Herman, S.W., Bermúdez, A., Delpino, D., 2001. Hydrothermal element fluxes from Copahue, Argentina: a ''beehive'' volcano in turmoil. Geology 29 (11), 1059–1062.

Vera, F.E., 2018. Origen, transporte y emplazamiento de lahares y avalanchas mixtas generadas en la erupción del 03 de marzo de 2015 en el volcán Villarrica, regiones de la Araucanía y Los Ríos, Chile. Thesis. Universidad de Concepción.

Waitt, R.B., Gardner, C.A., Pierson, T.C., Major, J.J., Neal, C.A., 1994. Unusual ice diamicts emplaced during the December 15, 1989 eruption of Redoubt Volcano, Alaska. J. Volcanol. Geoth. Res. 62, 409–428.

Waythomas, C.F., 2014. Water, ice and mud: lahars and lahar hazards at ice- and snowclad volcanoes. Geol. Today 30 (1), 34–39.

Waythomas, C.F., Pierson, T.C., Major, J.J., Scott, W.E., 2013. Voluminous ice-rich and water-rich lahars generated during the 2009 eruption of Redoubt Volcano, Alaska. J. Volcanol. Geoth. Res. 259, 389–413.

Waythomas, C.F., Haney, M.M., Fee, D., Schneider, D.J., Wech, A., 2014. The 2013 eruption of Pavlof Volcano, Alaska: a spatter eruption at an ice- and snow-clad volcano. Bull. Volcanol. 76, 862. https://doi.org/10.1007/s00445-014-0862-2.

White, J.D.L., Houghton, B.F., 2006. Primary volcaniclastic rocks. Geology 34, 677–680. https://doi.org/10.1130/G22346.1.

White, J.D.L., Riggs, N.R., 2001. Volcaniclastic sedimentation in lacustrine settings. Spec. Publs int. Ass. Sediment 30, 309.

Wilson, L., Head, J.W., 2002. Heat transfer and melting in subglacial basaltic volcanic eruptions: implications for volcanic deposit morphology and meltwater volumes. In: Smellie, J.L., Chapman, M.G. (Eds.), Volcano–ice Interaction on Earth and Mars, vol. 202. Geol. Soc. Spec. Pub., London, pp. 5–26.

Witham, C.S., 2005. Volcanic disasters and incidents: a new database. J. Volcanol. Geoth. Res. 148 (3–4), 191–233. https://doi.org/10.1016/j.jvolgeores.2005.04.017.

Wolff, J.A., Sumner, J.M., 2000. Lava Fountains and their products. In: Sigurdsson, H. (Ed.), Encyclopedia of Volcanoes. Academic Press, pp. 321–329.

Yasui, M., 2017. Textures of the Eruptive Products of Asama-Maekake Volcano from the 12th Century: Indicator of Eruptive Processes, vol. 53. Proceedings of the Institute of Natural Sciences, Nihon University, pp. 37–50.

Yasui, M., Koyaguchi, T., 2004. Sequence and eruptive style of the 1783 eruption of Asama Volcano, central Japan: a case study of an andesitic explosive eruption generating fountain-fed lava flow, pumice fall, scoria flow and forming a cone. Bull. Volcanol. 66, 243–262.